Glutamatergic calcium dynamics and deregulation of rat retinal ganglion cells

Andrew T. E. Hartwick[1,2], Claire M. Hamilton[1,2] and William H. Baldridge[1,2,3]

[1]*Retina and Optic Nerve Research Laboratory and the Departments of* [2]*Anatomy & Neurobiology and* [3]*Ophthalmology and Visual Sciences, Dalhousie University, Halifax, Nova Scotia, Canada*

A rise in intracellular calcium levels ($[Ca^{2+}]_i$) is a key trigger for the lethal effects of the excitatory neurotransmitter glutamate in various central neurons, but a consensus has not been reached on the pathways that mediate glutamate-dependent increases of $[Ca^{2+}]_i$ in retinal ganglion cells (RGCs). Using Ca^{2+} imaging techniques we demonstrated that, in the absence of external Mg^{2+}, the Ca^{2+} signal evoked by glutamate was predominantly mediated by NMDA-type glutamate receptors (NMDA-Rs) in immunopanned RGCs isolated from neonatal or adult rats. Voltage-gated Ca^{2+} channels and AMPA/kainate-Rs contributed a smaller portion of the Ca^{2+} response at saturating concentrations of glutamate. Consistent with NMDA-R involvement, extracellular Mg^{2+} inhibited RGC glutamate responses, while glycine had a potentiating effect. With Mg^{2+} present externally, the effect of AMPA/kainate-R antagonists was enhanced and both NMDA- and AMPA/kainate-R antagonists greatly reduced the glutamate-induced increases of RGC $[Ca^{2+}]_i$. This finding indicates that the primary contribution of AMPA/kainate-Rs to RGC glutamatergic Ca^{2+} dynamics is through the depolarization-dependent relief of the Mg^{2+} block of NMDA-R channels. The effect of glutamate receptor antagonists on glutamatergic Ca^{2+} signals from RGCs in adult rat retinal wholemounts yielded results similar to those obtained using immunopanned RGCs. Additional experiments on isolated RGCs revealed that during a 1 h glutamate (10–1000 μM) exposure, 18–28% of RGCs exhibited delayed Ca^{2+} deregulation (DCD) and the RGCs that underwent DCD were positive for the death marker annexin V. RGCs with larger glutamate-evoked Ca^{2+} signals were more likely to undergo DCD, and NMDA-R blockade significantly reduced the occurrence of DCD. Identifying the mechanisms underlying RGC excitotoxicity aids in our understanding of the pathophysiology of retinal ischaemia, and this work establishes a major role for NMDA-R-mediated increases in $[Ca^{2+}]_i$ in glutamate-related RGC death.

(Resubmitted 8 April 2008; accepted after revision 14 May 2008; first published online 15 May 2008)
Corresponding author W. H. Baldridge: Department of Anatomy & Neurobiology, Dalhousie University, Halifax, Nova Scotia, Canada B3H 1X5. Email: wbaldrid@dal.ca

The synaptic release of the excitatory neurotransmitter glutamate onto retinal ganglion cell (RGC) dendrites is an essential part of the visual pathway (reviewed by Thoreson & Witkovsky, 1999; Yang, 2004), but excessive or prolonged exposure to glutamate has long been considered lethal to these retinal output neurons (Lucas & Newhouse, 1957; Olney, 1969; Sisk & Kuwabara, 1985). While a rise in intracellular calcium levels ($[Ca^{2+}]_i$) is a key factor in the initiation of glutamate-related (excitotoxic) death of neurons throughout the CNS (see Sattler & Tymianski, 2000; Khodorov, 2004), the dynamics of altered $[Ca^{2+}]_i$ that occur in RGCs undergoing excitotoxic death have yet to be directly characterized.

This paper has online supplemental material.

N-Methyl-D-aspartate-type glutamate receptors (NMDA-Rs) are permeable to Ca^{2+} (Mayer & Westbrook, 1987; Ascher & Nowak, 1988) and, consistent with a role for NMDA-Rs in mediating excitotoxic RGC death, intravitreal injections of the selective agonist NMDA causes RGC loss in rodents *in vivo* (Siliprandi *et al.* 1992; Lam *et al.* 1999; Schlamp *et al.* 2001; Manabe *et al.* 2005; Nakazawa *et al.* 2005; Pernet *et al.* 2007; Reichstein *et al.* 2007). However, in addition to NMDA-Rs, rodent RGCs have also been shown to possess α-amino-3-hydroxy-5-methylisoxazole-4-propionate (AMPA) and kainate-type ionotropic glutamate receptors, based on electrophysiological recordings (Aizenman *et al.* 1988; Taschenberger *et al.* 1995; Chen & Diamond, 2002) and single-cell molecular profiling

 DOI: 10.1113/jphysiol.2008.154609

using RT-PCR (Jakobs *et al.* 2007). Although AMPA- and kainate-Rs are generally less permeable to Ca^{2+} than NMDA-Rs, AMPA-Rs that lack the GluR2 subunit are permeable to this cation (Jonas & Burnashev, 1995; Dingledine *et al.* 1999) and therefore this receptor subclass may also directly contribute to the glutamatergic Ca^{2+} responses of RGCs (see Osswald *et al.* 2007). Additionally, the indirect activation of voltage-gated Ca^{2+} channels (VGCCs), occurring after membrane depolarization due to NMDA-R and/or AMPA/kainate-R stimulation, could add to increases in RGC $[Ca^{2+}]_i$ (Ishida *et al.* 1991; Schubert & Akopian, 2004).

RGCs can be isolated into purified cultures using a Thy1 immunopanning technique (Barres *et al.* 1988; Meyer-Franke *et al.* 1995). This system should prove advantageous for assessing the relationships between glutamate, $[Ca^{2+}]_i$, and excitotoxicity in a central neuron as it eliminates the potential for the modulation of glutamatergic responses by neuroactive compounds released by other cells present in mixed cultures or intact tissue preparations. For example, treatment of mixed retinal cultures (in which RGCs make up $< 1\%$ of the cell population) with kainate causes an endogenous release of glutamate that contributes to the effect of kainate on RGCs (Sucher *et al.* 1991). However, investigations of excitotoxic death in purified RGC cultures have generated conflicting data that contradict previous *in vivo* studies (described above) linking NMDA-Rs to RGC death. Otori *et al.* (1998) reported that glutamate-induced Ca^{2+} influx and excitotoxicity occurs in immunopanned RGCs through activation of AMPA/kainate-Rs (due to similar pharmacology, AMPA- and kainate-Rs are often grouped together) rather than NMDA-Rs. In contrast, the findings of Ullian *et al.* (2004) suggest that RGCs in purified cultures, although expressing functional NMDA-Rs, are invulnerable to the excitotoxic actions of glutamate, NMDA or kainate. In light of these discrepancies, the goal of this work was to investigate the underlying pathways of Ca^{2+} entry that contribute to glutamatergic Ca^{2+} responses in RGCs and to investigate the relationship of $[Ca^{2+}]_i$ to excitotoxic RGC death.

Methods

Purified RGC cultures

All procedures were performed in accordance with the Dalhousie University Committee for the Use of Laboratory Animals. Unless noted otherwise, chemicals were obtained from Sigma-Aldrich (Oakville, ON, Canada). Natural litters of Long–Evans rats (Charles River, Montreal, QC, Canada) were killed at age 7–8 days postnatal by over-exposure to halothane vapours and decapitation. Following enucleation, the retinas were dissected from the eyes in Hibernate-A medium (BrainBits, Springfield, IL, USA) with 2% B27 supplements (Invitrogen, Burlington, ON, USA) and 10 μg ml^{-1} gentamicin. The retinas were incubated for 30 min at 37°C in 10 ml Ca^{2+}/Mg^{2+}-free Dulbecco's phosphate-buffered saline (DPBS; Invitrogen) containing 165 units of papain (Worthington Biochemicals, Lakewood, NJ, USA), 1 mM L-cysteine, and 0.004% DNase, and then mechanically triturated in an enzyme inhibitor solution of DPBS (with Ca^{2+} and Mg^{2+}) containing 1.5 mg ml^{-1} ovomucoid (Roche Diagnostics, Laval, QC, Canada), 1.5 mg ml^{-1} bovine serum albumin (BSA), and 0.004% DNase. The suspension was centrifuged (200 g for 11 min at 25°C) and then washed in DPBS containing higher concentrations (10 mg ml^{-1}) of ovomucoid and BSA. After spinning down, the cells were resuspended in DPBS containing 0.2 mg ml^{-1} BSA and 5 μg ml^{-1} insulin prior to incubation on the panning plates. In some experiments, RGC cultures were instead generated from adult Long–Evans rats that were 6–15 weeks old (3–4 rats per culture). Following dissection, the adult rat retinas were dissociated using the same methodology as for neonatal retinas except that a 60 min incubation period in papain solution was applied prior to trituration due to the more extensive synaptic connections in these aged retinas.

Purified RGC cultures (produced from either neonatal or adult retinas) were generated from the dissociated cell suspensions, as in previous work (see Hartwick *et al.* 2004, 2005 for details), using a two-step Thy1.1-based immunopanning procedure that was described originally by Barres *et al.* (1988). The immunopanned RGCs were plated onto poly D-lysine/laminin-coated Biocoat glass coverslips (12 mm; BD Biosciences, Bedford, MA, USA) in four-well tissue culture plates at a density of 3.5×10^4 cells per well. The cells were cultured in 600 μl of serum-free culture medium consisting of Neurobasal-A with 2% B27 supplements, 1 mM glutamine, 50 ng ml^{-1} brain-derived neurotrophic factor (BDNF), 10 ng ml^{-1} ciliary neurotrophic factor (CNTF) (BDNF and CNTF were generously provided by Regeneron, Tarrytown, NY, USA), 5 μM forskolin, and 10 μg ml^{-1} gentamicin. Cultures were maintained at 37°C in a humidified 5% CO_2–air atmosphere. For Ca^{2+} imaging, coverslips with plated cells were removed from the culture medium and incubated at 37°C for 30 min in a solution containing esterfied Ca^{2+} indicator dye (5 μM fura-2 AM or fura-4F AM, depending on the experiment; both from Invitrogen). The fura dyes were first dissolved in dimethyl sulfoxide (0.1% final concentration) and then solubilized in Hanks' balanced salt solution (HBSS) with 0.1% pluronic acid F-127 (Invitrogen).

Retinal wholemount preparation

Retinal wholemounts were prepared from adult Long–Evans rats aged 6–10 weeks and RGCs were loaded

with M_r 10 000 dextran-conjugated fura Ca^{2+} indicator dye (10% wt/vol, dissolved in purified water; Invitrogen). The rats were killed by over-exposure to halothane followed by decapitation. The eyes were enucleated, the anterior segment removed, and the posterior eye-cups were immersed in Hibernate-A medium with 2% B27 supplements for the retina dissection. Each retina was carefully dissected and mounted on black filters (HABP 045; Millipore, Bedford, MA, USA) with the RGC layer uppermost. A small volume (~0.5 μl) of the fura dextran was deposited into each retinal wholemount (passing through all the retinal layers) using a tapered 26-gauge needle fitted to a 10 μl syringe (Hamilton, Reno, NV, USA). To allow the dextran to be retrogradely transported to RGC somata, the wholemounts were then incubated in the dark at room temperature in Hibernate-A/B27 medium for 7–12 h prior to Ca^{2+} imaging. Further details on the technique of loading RGCs in retinal wholemounts with fura dextran are described in previous work (Baldridge, 1996; Hartwick *et al.* 2005).

Calcium imaging

Following fura dye loading, the isolated RGCs (on coverslips) or retinal wholemounts (on filters) were transferred to a microscope chamber that was constantly superfused with 100% oxygen-bubbled HBSS. The HBSS was warmed to 34–35°C and delivered by a peristaltic pump to the chamber at a flow rate of approximately 1 ml min^{-1}. In most experiments, the HBSS (pH 7.4) was modified to be nominally free of magnesium ions (Mg^{2+}) and contained 2.6 mM $CaCl_2$ and 15 mM Hepes buffer. For experiments testing the effect of extracellular Mg^{2+}, $MgCl_2$ was substituted for some of the $CaCl_2$ so that the final divalent concentrations were 0.8 mM Mg^{2+} and 1.8 mM Ca^{2+}, unless specified otherwise. The fura-loaded RGCs were alternately stimulated with 340 and 380 nm light, with a period of excitation for each wavelength of 1000–1500 ms for the retinal wholemounts and 400 ms for the isolated cells. During treatments, image pairs were collected as often as every 5 s (10 s for retinal wholemounts) but to limit photodamage, images were collected less frequently (20–40 s) during intervening periods. Details on the microscope rig and related apparatus used for calcium imaging have been described in previous work (Hartwick *et al.* 2004; Hartwick *et al.* 2005). The fluorescence images (8-bit processing, 4 × 4 binning) were converted into ratiometric (340 nm/380 nm) data by imaging software (Imaging Workbench 2.2, Axon Instruments, Union City, CA, USA).

Glutamatergic Ca^{2+} dynamics were assessed in the isolated RGCs using two treatment paradigms. RGCs were either exposed to glutamate receptor agonists (glutamate, glycine, NMDA, kainate; all dissolved directly in HBSS on the day of the experiment; kainate was obtained from Tocris, Ellisville, MO, USA) for a relatively brief 30 s pulse, or were treated with glutamate/glycine for a prolonged 1 h period. RGCs in the 30 s treatment experiments were loaded with high affinity fura-2 AM (K_D ~224 nM) dye, while RGCs exposed to glutamate for 1 h were loaded with low affinity fura-4F AM (K_D ~770 nM) dye. For fura dextran-loaded RGCs in retinal wholemounts, the treatment period with glutamatergic agonists was 2 min and the glutamate transporter inhibitor DL-threo-β-benzyloxyaspartate (TBOA; Tocris) was added to the glutamate treatment solution. In both prolonged glutamate exposure experiments on isolated RGCs and experiments on retinal wholemounts, the imaging rig was modified in that a 0.6× coupling tube (HRP060; Diagnostic Instruments, Sterling Heights, MI, USA) was placed between the CCD camera and microscope to expand the field of view afforded by the 40× objective.

Imaging analysis

For studies on isolated RGCs, circular regions of interest were drawn around individual RGC somata, and the mean fura ratio within each region was monitored throughout the experiments. Background fluorescence was measured from a region on the coverslip devoid of RGCs and subtracted from each image. For the experiments in which isolated RGCs were exposed to glutamate for 30 s pulses, the fura-2 ratios (R) were converted to $[Ca^{2+}]_i$ using the formula:

$$[Ca^{2+}]_i = K_d(F_o/F_s)[(R - R_{min})/(R_{max} - R)]$$

with a K_d for fura-2 of 224 nM, and where F_o/F_s is the ratio of fluorescence intensity at 380 nm excitation in Ca^{2+}-free solution over the intensity in solution with saturated Ca^{2+} levels (Grynkiewicz *et al.* 1985; Kao, 1994). A sample ($n = 5$–15) of the isolated RGCs in a given imaging session were superfused first with Ca^{2+}-free HBSS (10 mM Mg^{2+}, 2 mM BAPTA, 10 μM ionomycin) to determine the minimum value for the fura-2 ratio (R_{min}), and then with saturating Ca^{2+} solution (0.9% saline with 20 mM Ca^{2+}, 10 μM ionomycin) to determine the maximum fura-2 ratio (R_{max}). Mean values for F_o/F_s, R_{min} and R_{max} were calculated from these RGCs and used to convert the fura-2 ratios for other RGCs in the imaging session to $[Ca^{2+}]_i$. The variability in these values from different imaging sessions was relatively minor; for 10 consecutive calibration experiments, the mean R_{min} was 0.26 ± 0.03 (S.D.) and the mean R_{max} was 2.57 ± 0.12 (S.D.). Ca^{2+} influx was measured as the peak $[Ca^{2+}]_i$ obtained following each treatment (with glutamate or related agonists) minus the average baseline $[Ca^{2+}]_i$ measured prior to the first treatment. In trials assessing the effect of glutamate receptor antagonists and VGCC blockers, RGCs that had a negligible response to glutamate

(peak $[Ca^{2+}]_i < 150$ nM) were excluded from analysis. In the prolonged glutamate exposure (1 h) experiments, the initial Ca^{2+} influx (Δfura-4F ratio) was measured as the peak fura-4F ratio occurring during the first 400 s of the glutamate treatment minus the average baseline ratio prior to treatment.

For studies on RGCs in retinal wholemounts, the mean fura ratio was monitored in RGC somata that exhibited fluorescence with 380 nm excitation. As in previous work (Hartwick *et al.* 2005), all experiments were performed on dextran-loaded cell bodies that were located in the GCL near labelled RGC axon bundles, and that were $> 200\ \mu$m from the dextran injection site to ensure that imaged cells were RGCs. The response to each treatment was calculated as the Δfura ratio, the peak fura ratio minus baseline fura ratio. The baseline fura ratio for every cell was calculated as the average fura ratio measured in the three images prior to each treatment, and the peak ratio was the maximum ratio value obtained in the 400 s following each treatment. For illustration, fura ratio traces of RGCs from retinal wholemounts were slope-corrected for a gradual decrease in baseline ratio due to decreasing background fluorescence. All data analysis was performed on the non-baseline-corrected raw data. Data from either isolated RGCs or retinal wholemount preparations are presented as means $\pm$ S.D.

RGC death assay

After the 1 h glutamate exposure, RGCs were imaged for another 15 min to monitor for recovery. The superfusing HBSS was then stopped and 5 μl of fluorescently tagged annexin V (Alexa Fluor 488 annexin V; Invitrogen) was added to the microscope chamber (chamber volume $\sim$0.5 ml) to compare the Ca^{2+} imaging data with a marker of cell death. After 10 min incubation, the flow of HBSS was resumed for 5 min to wash. Images of annexin V fluorescence were captured with the CCD camera using an FITC filter set (XF100 set; excitation 475 nm, emission 535 nm; dichroic 505 nm; Omega Optical) and saved, through the imaging software program, with and without the circular regions of interest that had been drawn for Ca^{2+} imaging. Annexin V fluorescence was assessed using Photoshop 5.0 software (Adobe Systems, San Jose, CA, USA). Using the histogram function, a cell was deemed annexin V positive if the mean luminance minus 1 S.D. within its outlined region of interest was greater than background luminance in a section devoid of cells.

Results

Glutamatergic Ca^{2+} dynamics of neonatal rat RGCs

Ca^{2+} imaging experiments were performed on cultured RGCs 1–3 days after their isolation through Thy1-based immunopanning. Upon loading of fura-2 Ca^{2+} indicator dye, the isolated RGCs typically displayed a bi-lobed pattern of fluorescence, under either 340 or 380 nm excitation, presumably due to an asymmetrical nucleus position (Fig. 1*A*). To investigate the relationship of glutamate concentrations to Ca^{2+} responses, isolated RGCs ($n = 38$; pooled from 8 imaging experiments on RGCs from 3 separate cultures) were challenged with 30 s treatments of 1, 10, 50 and 100 μM glutamate (example trace in Fig. 1*D*). Glycine (10 μM), a coagonist with glutamate for NMDA-Rs (Johnson & Ascher, 1987), was included in all glutamate treatment solutions, and the superfusing HBSS was nominally Mg^{2+}-free. The mean changes (peak response minus baseline) in fura-2 fluorescence ratios (340/380 nm; measured in RGC somata; Fig. 1*B* and *C*) induced by the different glutamate concentrations are shown in Fig. 1*E*. The ratiometric data from these experiments (and in subsequent fura-2 imaging experiments on the isolated cells) were also converted to absolute $[Ca^{2+}]_i$ (see Methods for calibration details) to give an approximation of the magnitude of the rise in $[Ca^{2+}]_i$ caused by the glutamate treatments (Fig. 1*E*). The responses to the four different glutamate concentrations were all significantly different from each other ($P < 0.01$, Friedman ANOVA, Tukey; using either Δfura-2 ratio or $\Delta[Ca^{2+}]_i$ data) with the exception of 50 *versus* 100 μM ($P > 0.05$), indicating that 50 μM glutamate was sufficient to evoke the maximum Ca^{2+} response. During the 1 μM glutamate treatments, there was negligible alteration in $[Ca^{2+}]_i$ from baseline levels (rise of 35 nM $\pm$ 37 from a mean baseline $[Ca^{2+}]_i$ of 70 nM $\pm$ 24), signifying that this concentration was below the threshold required to consistently elicit a response under our recording conditions. The rises in $[Ca^{2+}]_i$ produced by the 10 μM glutamate exposures were, on average, roughly one-half (51.9% $\pm$ 25.2; within-cell analysis) of those elicited by the saturating 100 μM glutamate treatments.

In addition to glutamate, increases in RGC $[Ca^{2+}]_i$ also occurred following application of either NMDA or kainate, selective ligands for NMDA-Rs and AMPA/kainate-Rs, respectively (Fig. 2). In a direct comparison of the Ca^{2+} signal induced by 200 μM NMDA (with 10 μM glycine) to that by increasing concentrations of kainate in isolated RGCs ($n = 33$), the magnitude of NMDA-induced Ca^{2+} influx (363 nM $\pm$ 357) was similar ($P > 0.05$, $q = 0.202$, Friedman ANOVA, Tukey) to that due to 200 μM kainate (398 nM $\pm$ 499) but was significantly ($P < 0.01$) greater and smaller than the responses elicited by 100 μM (104 $\pm$ 189 nM) and 300 μM (907 $\pm$ 786 nM) kainate, respectively (example trace in Fig. 2*A*). As expected, RGC responses to NMDA were highly dependent on the presence of the NMDA-R coagonist glycine in the treatment solution (Fig. 2*B*). The RGC Ca^{2+} signals stimulated by 200 μM NMDA alone were significantly less ($P < 0.001$, Wilcoxon) than the signal produced by 200 μM NMDA plus 10 μM glycine (in $n = 34$ RGCs,

the normalized NMDA-induced $\Delta[Ca^{2+}]_i$ was only $25.3 \pm 11.9\%$ of the same RGCs' response to NMDA plus glycine), but glycine did not significantly ($P = 0.134$, Wilcoxon) enhance kainate responses ($n = 19$ RGCs treated with 200 μM kainate alone and then 200 μM kainate plus 10 μM glycine). In addition to Ca^{2+} influx linked to ionotropic glutamate receptors, the stimulation of group I metabotropic glutamate receptors (mGluR) can produce a rise in $[Ca^{2+}]_i$ in many CNS neurons (Linden *et al.* 1994; Guatteo *et al.* 1999). However, the selective group I mGluR agonist (*S*)-3,5-dihydroxyphenylglycine hydrate (DHPG) had no direct effect on the $[Ca^{2+}]_i$ of the immunopanned RGCs (Fig. 2*C*; representative of $n = 15$ RGCs tested), and therefore we focused on ionotropic glutamate receptors for the remainder of the study.

Mechanisms of glutamate-induced Ca^{2+} influx in isolated RGCs

The experiments with the glutamatergic agonists NMDA and kainate confirmed that there are at least two distinct pathways through which glutamate could potentially influence RGC $[Ca^{2+}]_i$. Glutamate is the natural endogenous ligand for glutamate receptors, and its action can differ from that of its related agonists. In particular, the activation of AMPA-Rs by glutamate is accompanied by rapid desensitization, but this desensitization is markedly reduced if AMPA-Rs are instead stimulated with kainate (Dingledine *et al.* 1999). Therefore, the magnitude of kainate-induced Ca^{2+} influx may be exaggerated, as compared to that mediated by glutamate stimulation of AMPA/kainate-Rs.

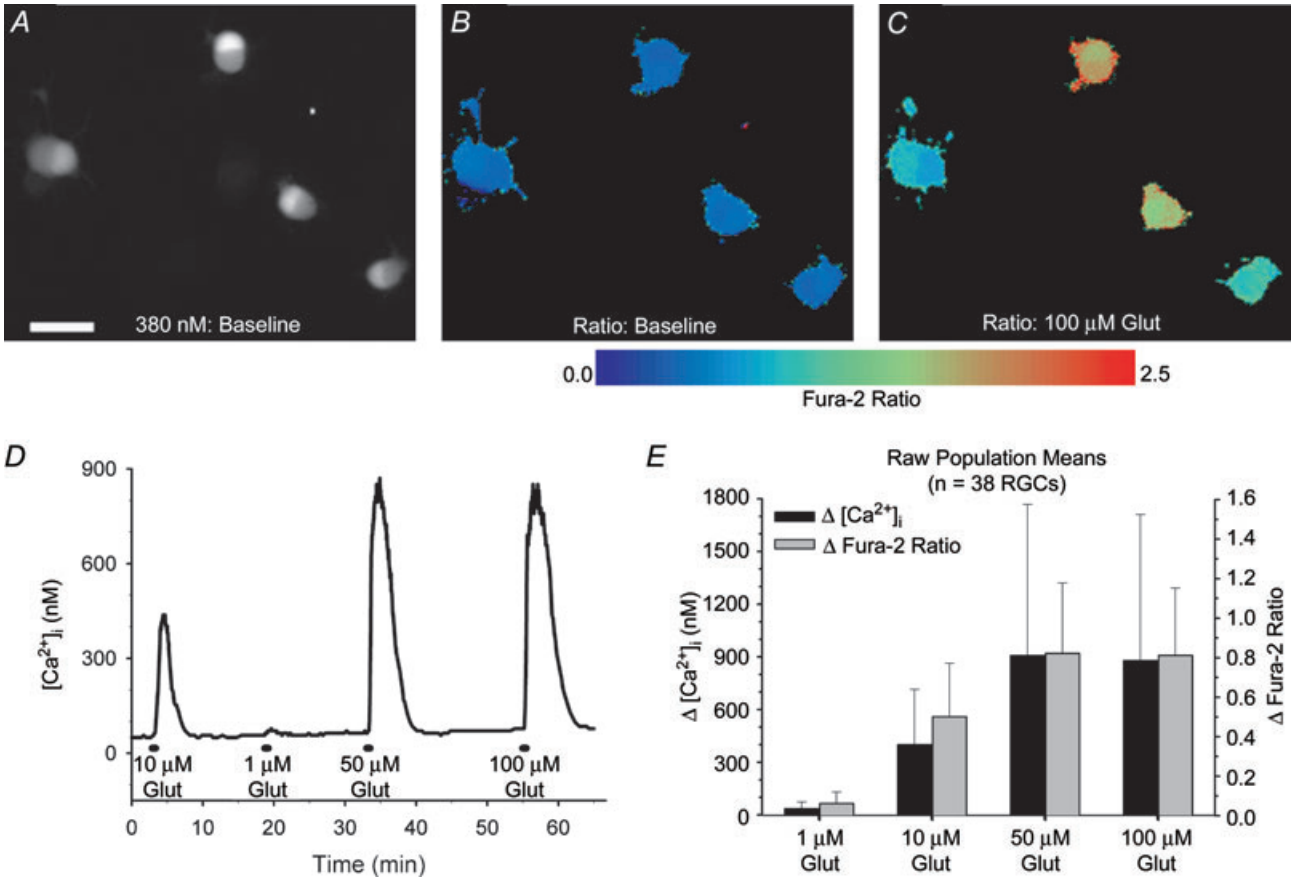

Figure 1. Concentration–response relationship for glutamate-induced increases of $[Ca^{2+}]_i$ in cultured RGCs isolated from neonatal rats

A, fluorescence (380 nm excitation, 510 nm emission) of immunopanned RGCs loaded with the Ca^{2+} indicator dye fura-2 AM. Scale bar = 25 μm. *B* and *C*, pseudocolour images of fura-2 fluorescence ratios (340/380 nm) in same RGCs at baseline (*B*) and at peak response to 100 μM glutamate (*C*). *D*, example trace (fura-2 ratios converted to $[Ca^{2+}]_i$) from an isolated RGC exposed for 30 s to 1, 10, 50 and 100 μM glutamate (plus 10 μM glycine; extracellular Mg^{2+} absent). *E*, summary of mean (±1 S.D.; $n = 38$ RGCs) responses produced by the glutamate treatments. Both the $\Delta[Ca^{2+}]_i$ and the Δfura-2 ratios (peak response minus baseline) are shown.

To test the relative contribution of NMDA-R and AMPA/kainate-R-mediated pathways, we assessed the effect of the respective antagonists D(−)-2-amino-5-phosphonopentanoic acid (APV) and 2,3-dihydro-6-nitro-7-sulfamoyl-benzo(f)quinoxaline (NBQX) on the Ca^{2+} signal produced by a 30 s treatment of 10 and 100 μM glutamate (plus 10 μM glycine). These concentrations were chosen because, as shown in Fig. 1, they elicited the near-threshold (10 μM) and maximum (100 μM) Ca^{2+} responses in the isolated RGCs in Mg^{2+}-free conditions. NBQX was used as the AMPA/kainate-R antagonist because it was observed in initial experiments that the related quinoxalines 6,7-dinitroquinoxaline-2,3-dione (DNQX) and 6-cyano-7-nitroquinoxaline-2,3-dione (CNQX) quenched fura-2 fluorescence and absorbed light preferentially at 340 nm relative to 380 nm. Unlike DNQX and CNQX at the same concentration, 25 μM NBQX did not artificially alter the ratiometric data (see online Supplemental material).

The NMDA-R antagonist APV (100 μM) greatly ($P < 0.01$, Friedman ANOVA, Tukey; as compared to both initial and recovery responses with APV absent) reduced the $[Ca^{2+}]_i$ elevation that occurred with either 10 or 100 μM glutamate treatment (Fig. 3*A*, *C* and *D*). The AMPA/kainate-R antagonist NBQX (25 μM) did not affect ($P = 0.418$, Friedman ANOVA) RGC responses to 10 μM glutamate, but it did have a small yet significant ($P < 0.01$, Friedman ANOVA, Tukey) effect on 100 μM glutamate responses (Fig. 3*B*, *C* and *D*). These results indicate that glutamate-induced Ca^{2+} influx occurs predominantly through NMDA-R activation, although at higher glutamate concentrations there is a small AMPA/kainate-R contribution. Glycine was included in the glutamate treatment solutions because it is a coagonist with glutamate at NMDA-Rs (Johnson & Ascher, 1987), and there is evidence that endogenous retinal levels of glycine or D-serine sufficiently activate the glycine binding site of RGC NMDA-Rs *in vivo* (Hama *et al.* 2006). While glycine had no effect on RGC $[Ca^{2+}]_i$ on its own, the addition of glycine to the glutamate solutions significantly ($P < 0.05$, Friedman ANOVA, Tukey) enhanced RGC responses (Fig. 3*E* and *F*), and this is consistent with NMDA-Rs mediating the glutamate-related rise in RGC $[Ca^{2+}]_i$.

We next sought to assess the contribution of VGCCs to glutamate-evoked changes in $[Ca^{2+}]_i$, as Ca^{2+} could also pass through these channels following the RGC membrane depolarization induced by glutamate treatment. We first attempted to inhibit all VGCC types with the non-selective blocker cadmium, but this divalent cation interfered with the fura-2 dye (data not shown). Instead, RGCs were stimulated with glutamate, NMDA or kainate in the presence of 5 μM ω-conotoxin GVIA plus 10 μM verapamil, concentrations that have been shown to inhibit N- and L- type ($Ca_V2.2$ and Ca_V1 of more recent nomenclature) VGCCs, respectively, in isolated cells (Freedman *et al.* 1984; Boland *et al.* 1994). Verapamil was used rather than the L-type VGCC blocker nifedipine, because the latter compound absorbed asymmetrically at the 340 and 380 nm excitation wavelengths (see Supplemental material for illustration of the effect of asymmetrical fluorescence quenching on fura-2 ratiometric Ca^{2+} imaging). It has previously been shown that 10 μM verapamil significantly reduced the overall change in intracellular Ca^{2+} in isolated rat retinas exposed to NMDA (Melena & Osborne, 2001).

The VGCC blocking cocktail of verapamil and ω-conotoxin GVIA significantly ($P < 0.05$, Friedman ANOVA, Tukey) reduced the Ca^{2+} influx induced by either 100 μM glutamate or 200 μM kainate, but did not ($P > 0.05$) alter RGC responses to 10 μM glutamate or 200 μM NMDA (Fig. 4). These results suggest that VGCCs are not involved in Ca^{2+} signals produced by a near-threshold glutamate dose (10 μM), but

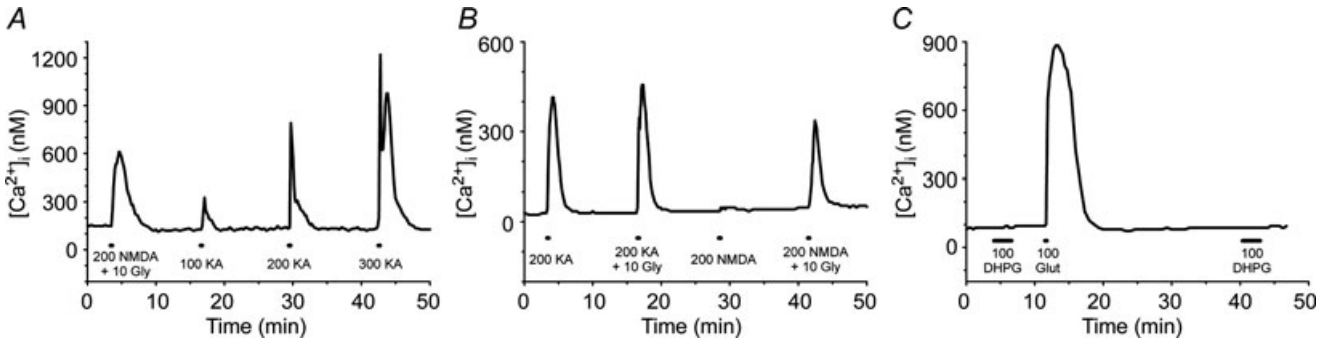

Figure 2. NMDA- and kainate-induced Ca^{2+} influx in isolated RGCs
A, example fura-2 ratio trace for an RGC treated with 200 μM NMDA plus 10 μM glycine, and then 100, 200 and 300 μM kainate. *B*, glycine (10 μM) significantly enhanced the response evoked by 200 μM NMDA, but not 200 μM kainate. *C*, in contrast to glutamate, NMDA or kainate, the metabotropic glutamate receptor agonist DHPG (100 μM) had no direct effect on RGC $[Ca^{2+}]_i$. Mg^{2+}-free HBSS was used as the extracellular solution.

these channels do contribute significantly to changes in $[Ca^{2+}]_i$ evoked by a saturating glutamate concentration (100 μM) in the isolated RGCs. A concentration of 200 μM was used for both NMDA and kainate, as these concentrations had been shown to elicit roughly equivalent Ca^{2+} signals (see Fig. 2*A*). In accord, the mean magnitude of Ca^{2+} responses evoked by 200 μM kainate was not significantly different ($P = 0.91$, *t* test) from the magnitude of responses produced by 200 μM NMDA (with 10 μM glycine) treatment. These results indicate a greater role for VGCCs in AMPA/kainate-R-mediated Ca^{2+} signals relative to comparable NMDA-R-drive responses.

The superfusing HBSS used in all Ca^{2+} imaging experiments presented so far was nominally Mg^{2+}-free.

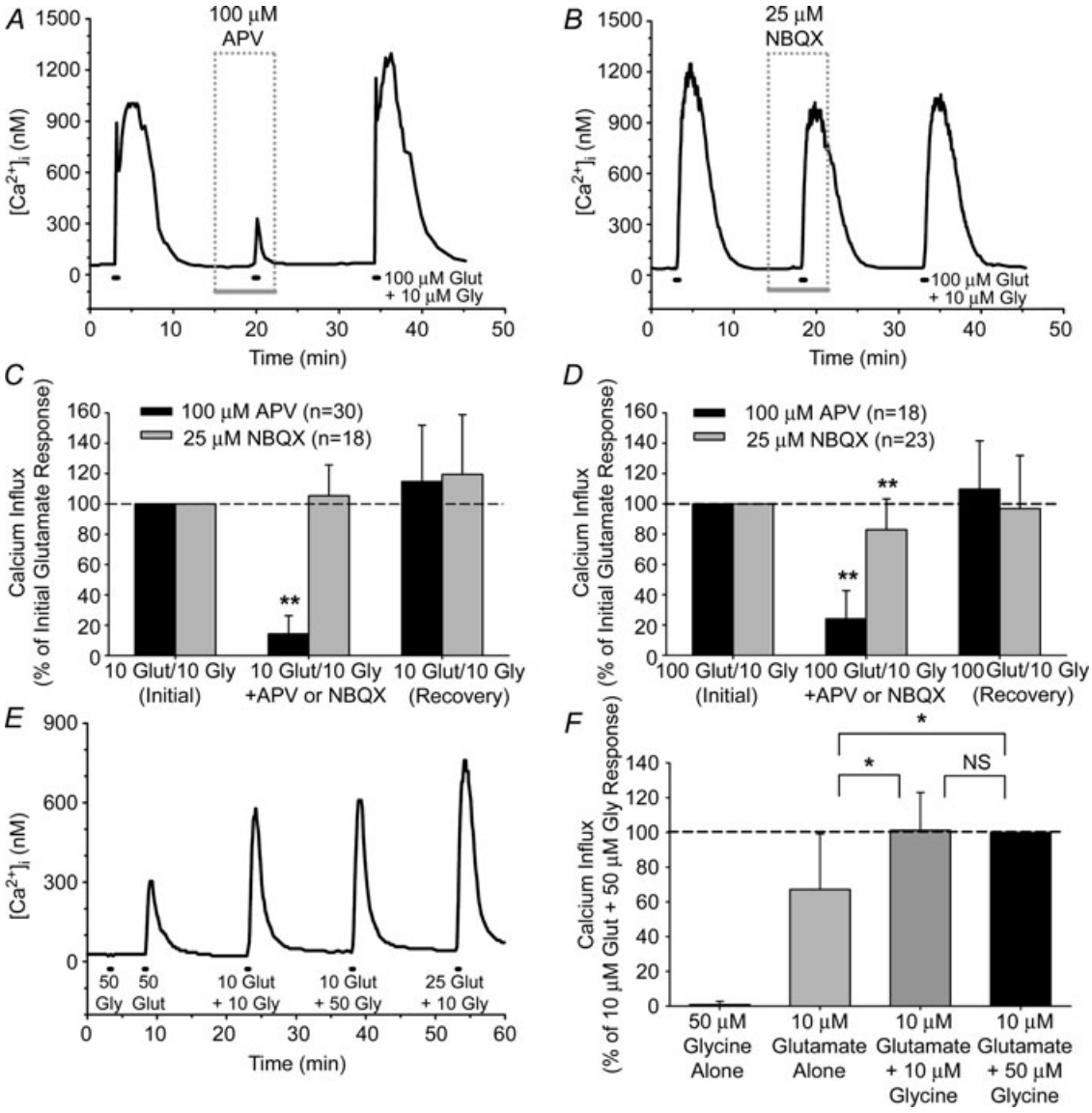

Figure 3. Effect of glutamate (Glut) receptor antagonists and glycine (Gly) on glutamate-induced Ca^{2+} influx in isolated RGCs

A and *B*, example fura-2 ratio traces illustrating effects of NMDA-R antagonist APV (*A*) and AMPA/kainate-R antagonist NBQX (*B*) on Ca^{2+} signals evoked by 100 μM Glut. *C* and *D*, mean data (+1 S.D.) showing effect of antagonists on Ca^{2+} influx due to 10 μM (*C*) and 100 μM (*D*) Glut treatments (with 10 μM Gly; extracellular Mg^{2+} absent). Ca^{2+} influx in these experiments was calculated as the change in $[Ca^{2+}]_i$, following conversion of the fura-2 ratios through calibration experiments, and the data was normalized to initial RGC glutamate responses (dashed line). *E* and *F*, example fura-2 ratio trace (*E*) and mean normalized data (+1 S.D.) (*F*) summarizing effect of 50 μM Gly alone, 10 μM Glut alone, 10 μM Glut plus 10 μM Gly, and 10 μM Glut plus 50 μM Gly on RGCs ($n = 14$). Gly alone did not affect $[Ca^{2+}]_i$, but potentiated RGC responses to Glut. $^*P < 0.05$, $^{**}P < 0.01$, Friedman ANOVA, Tukey, within-cell comparisons on normalized data.

Mg^{2+} is known to exert a voltage-dependent block of the NMDA-R channel pore (Mayer *et al.* 1984; Nowak *et al.* 1984). In the presence of 0.8 mM Mg^{2+}, the magnitude of the Ca^{2+} signal induced by various glutamate concentrations was blunted as compared to recordings in Mg^{2+}-free HBSS, with 10 and 100 μM glutamate often being below threshold (example trace in Fig. 5*A*; compare to Fig. 1*D*). To directly test the effect of extracellular Mg^{2+}, isolated RGCs ($n = 12$) were exposed to consecutive glutamate treatments (10 μM; with 10 μM glycine) while the superfusing solution alternated between Mg^{2+}-free HBSS and HBSS containing 0.8 mM Mg^{2+} (Fig. 5*B*). Glutamate-induced Ca^{2+} influx was significantly diminished ($P < 0.01$, Friedman ANOVA, Tukey) with extracellular Mg^{2+} present as compared to initial and recovery responses in Mg^{2+}-free HBSS (Fig. 5*C*). In these experiments, the concentration of Ca^{2+} was reduced in the Mg^{2+}-containing HBSS in order to keep the overall divalent cation levels constant. To control for the possibility that it was the decreased Ca^{2+}, rather than the presence of Mg^{2+}, that caused the reduction in the glutamate-induced Ca^{2+} responses, we performed additional control experiments in which only the Ca^{2+} concentration of the external solution was varied. RGC responses to 10 μM glutamate (with glycine) in Mg^{2+}-free HBSS containing 1.8 mM Ca^{2+} were 95 ± 36% ($n = 49$; within-cell analysis) of those obtained after switching the cells to Mg^{2+}-free HBSS containing 2.6 mM Ca^{2+}, and were not significantly different ($P > 0.05$, Wilcoxon). Thus, the reduction in the RGC glutamate responses illustrated in Fig. 5*A–C* was directly due to the addition of extracellular Mg^{2+}.

The effects of glutamate receptor antagonists were then re-assessed on RGCs challenged with 1000 μM glutamate with 0.8 mM Mg^{2+} present. Only RGCs exhibiting a $\Delta[Ca^{2+}]_i$ of at least 150 nM (roughly equivalent to a Δfura-2 ratio of 0.2) due to glutamate treatment were included in analysis. Under these

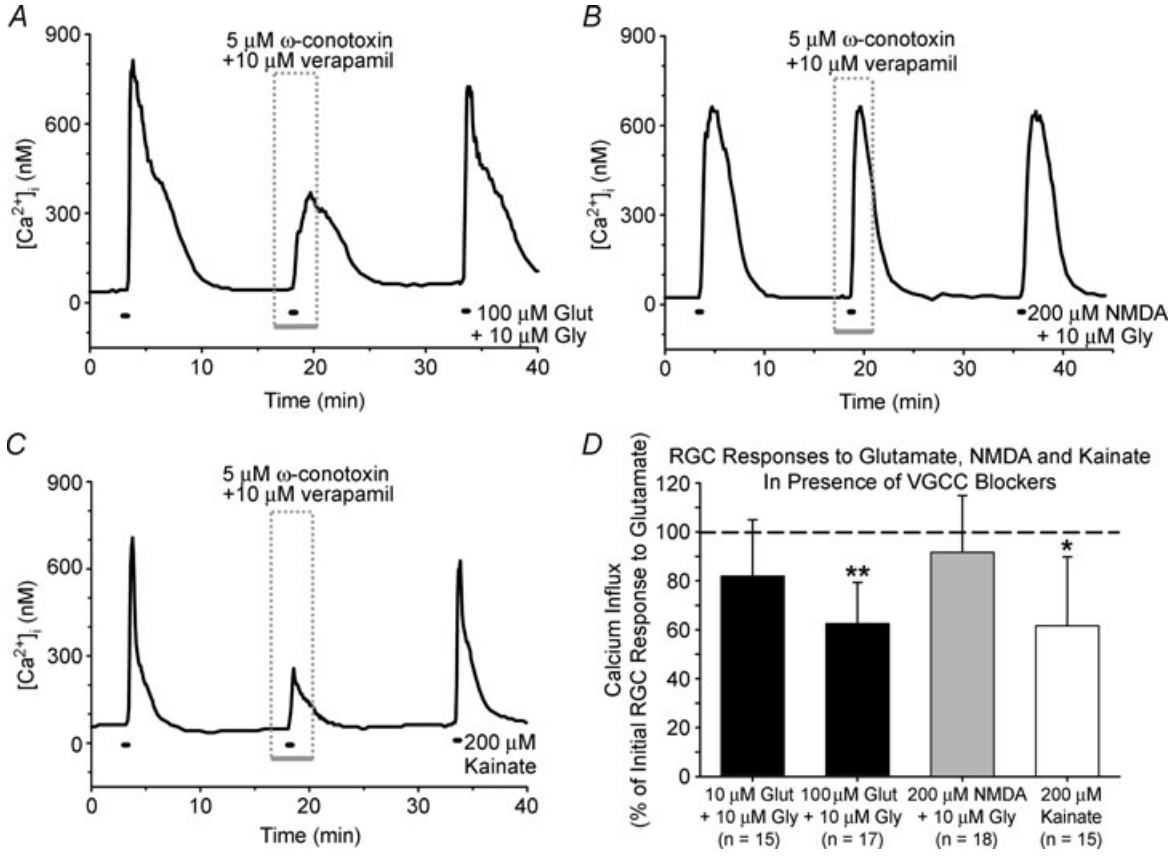

Figure 4. Effect of voltage-gated Ca^{2+} channel (VGCC) inhibition on glutamatergic RGC Ca^{2+} influx
A–C, representative fura-2 ratio traces for RGCs treated with 100 μM glutamate (*A*), 200 μM NMDA (*B*) and 200 μM kainate (*C*) in the presence or absence of 5 μM ω-conotoxin GVIA and 10 μM verapamil. *D*, mean data (+1 S.D.) showing effects of VGCC blocking cocktail on Ca^{2+} influx induced by 10 μM and 100 μM glutamate, 200 μM NMDA and 200 μM kainate (extracellular Mg^{2+} absent; 10 μM glycine added to glutamate and NMDA solutions). Ca^{2+} influx was the change in $[Ca^{2+}]_i$ due to treatment, and was normalized to the initial glutamate, NMDA or kainate responses (dashed line). $^*P < 0.05$, $^{**}P < 0.01$, Friedman ANOVA, Tukey, compared to initial and recovery responses.

conditions, the AMPA-kainate-R antagonist NBQX (25 μM) reduced ($P < 0.01$, Friedman ANOVA, Tukey) the glutamate-evoked Ca^{2+} signals (Fig. 5*E* and *F*). The NMDA-R antagonist APV, at 100 μM, had a small but significant ($P < 0.05$) effect (Fig. 5*F*). However, the effect of APV was greater at increasing concentrations (data not shown), suggesting that this competitive antagonist was being out-competed by the high (1000 μM) glutamate concentration. To confirm this hypothesis, we tested the non-competitive NMDA-R channel blocker MK-801 (10 μM), and found that this antagonist exhibited a strong inhibitory effect ($P < 0.01$; Fig. 5*D* and *F*). Therefore, in the presence of external Mg^{2+}, antagonism of either NMDA-Rs or AMPA/kainate-Rs resulted in near abolition of glutamate-induced Ca^{2+} influx.

Glutamate-induced Ca^{2+} influx in adult rat RGCs: isolated cells and retinal wholemounts

All preceding experiments were performed on purified RGC cultures generated from neonatal rats (age 7–8 postnatal days). At this age, RGC dendrites are just beginning to form functional glutamatergic synapses with retinal bipolar cells (Bansal *et al.* 2000; Wong *et al.* 2000), raising the possibility that RGC glutamate receptor expression in neonates differs from adults. Embryonic or early postnatal animals have traditionally been used for neuronal cultures, as the neurons at younger ages have not yet formed extensive synaptic connections and are generally thought to be less susceptible to damage during dissociation. To test whether the mechanisms underlying glutamate-induced

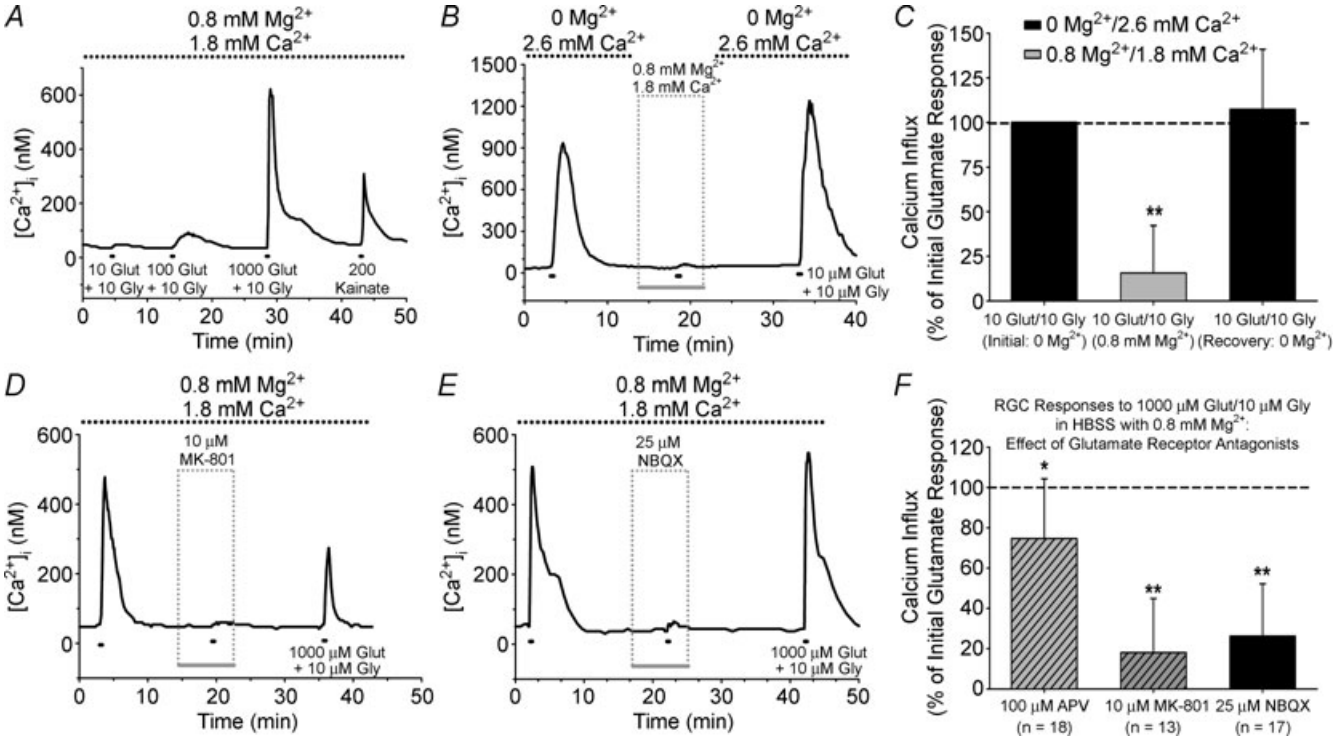

Figure 5. Effect of extracellular Mg^{2+} on glutamate-induced Ca^{2+} influx in isolated RGCs
A, fura-2 ratio trace for an RGC, in HBSS containing 0.8 mM Mg^{2+}, exposed to 10, 100 and 1000 μM glutamate (plus 10 μM glycine). Responses to lower glutamate concentrations ($\leq$ 100 μM) were attenuated with Mg^{2+} present, but note that RGC still responded to 200 μM kainate (indicating AMPA/kainate-Rs were not inhibited by the extracellular Mg^{2+}). *B* and *C*, representative trace (*B*) and mean normalized Ca^{2+} influx (change in $[Ca^{2+}]_i$ +1 S.D.) (*C*) for RGCs ($n = 12$) treated with 10 μM glutamate in the absence or presence of 0.8 mM Mg^{2+}. *D* and *E*, fura-2 ratio traces illustrating effect of NMDA-R antagonist MK-801 (10 μM) (*D*) and AMPA/kainate-R antagonist NBQX (25 μM) (*E*) on RGC Ca^{2+} influx evoked by 1000 μM glutamate (plus 10 μM glycine) in HBSS containing 0.8 mM Mg^{2+}. *F*, mean data (+1 S.D.) for effect of NMDA-R antagonists (hatched bars) and AMPA/kainate-R antagonist (filled bar) on glutamate-induced Ca^{2+} influx (normalized to initial response; dashed line). $^*P < 0.05$, $^{**}P < 0.01$, Friedman ANOVA, Tukey, compared to initial and recovery responses.

Ca^{2+} influx change as rats mature, purified RGC cultures were generated from adult rats (age 6–15 weeks) using the Thy1 immunopanning technique.

The yield of immunopanned RGCs extracted from adult retinas ranged between 10 000 and 17 000 RGCs per retina, as compared to 25 000–40 000 RGCs per retina for neonatal rats. This reduction is not due to developmental RGC loss as the total number of RGCs at age 7–8 days is roughly the same as in adult rats (Potts *et al.* 1982), but is likely to be due to the loss of more cells to damage during dissociation. In contrast to immunopanned RGCs from neonatal rats, RGCs isolated from adult rat retinas displayed little neurite outgrowth in culture (Fig. 6*A*). Despite this morphological difference, glutamate-induced Ca^{2+} influx (with glycine present and extracellular Mg^{2+} absent) was primarily mediated through NMDA-R activation in cultured adult RGCs as in neonatal RGCs. The NMDA-R antagonist APV (100 μM) significantly reduced ($P < 0.01$, Friedman ANOVA, Tukey, compared to both initial and recovery responses) the Ca^{2+} influx induced by 10 μM or 100 μM glutamate, while the AMPA/kainate-R antagonist NBQX had negligible ($P > 0.05$) effect (Fig. 6*B* and *C*). Also similar to the neonatal RGCs, the Ca^{2+} responses of isolated adult RGCs exposed to 10 μM glutamate were significantly ($P < 0.01$) reduced with 0.8 mM Mg^{2+} present (Fig. 6*C*; experimental protocol same as shown in Fig. 5*B*)

To determine whether the mechanisms underlying glutamatergic Ca^{2+} dynamics were altered by the dissociation procedure, we next tested the relative effectiveness of glutamate receptor antagonists on RGCs in retinal wholemounts prepared from adult rats. RGCs were retrogradely loaded with dextran-conjugated fura Ca^{2+} indicator dye (Fig. 7*A*) following injection of the dye into the filter-mounted retinas. Due to intercell differences in dye loading inherent with this technique (see Hartwick *et al.* 2005) and due to changing background fluorescence (attributed to the washing out of excess fura dextran that remained on the retinal surface from the injection), a valid calibration of the ratiometic data to absolute $[Ca^{2+}]_i$ was not possible and Ca^{2+} responses were measured as the raw changes in fura fluorescence ratios. As demonstrated in previous work (Hartwick *et al.* 2005), micromolar concentrations of glutamate were ineffective at stimulating an RGC Ca^{2+} response in this preparation. This is due to the efficiency of retinal glutamate uptake that quickly

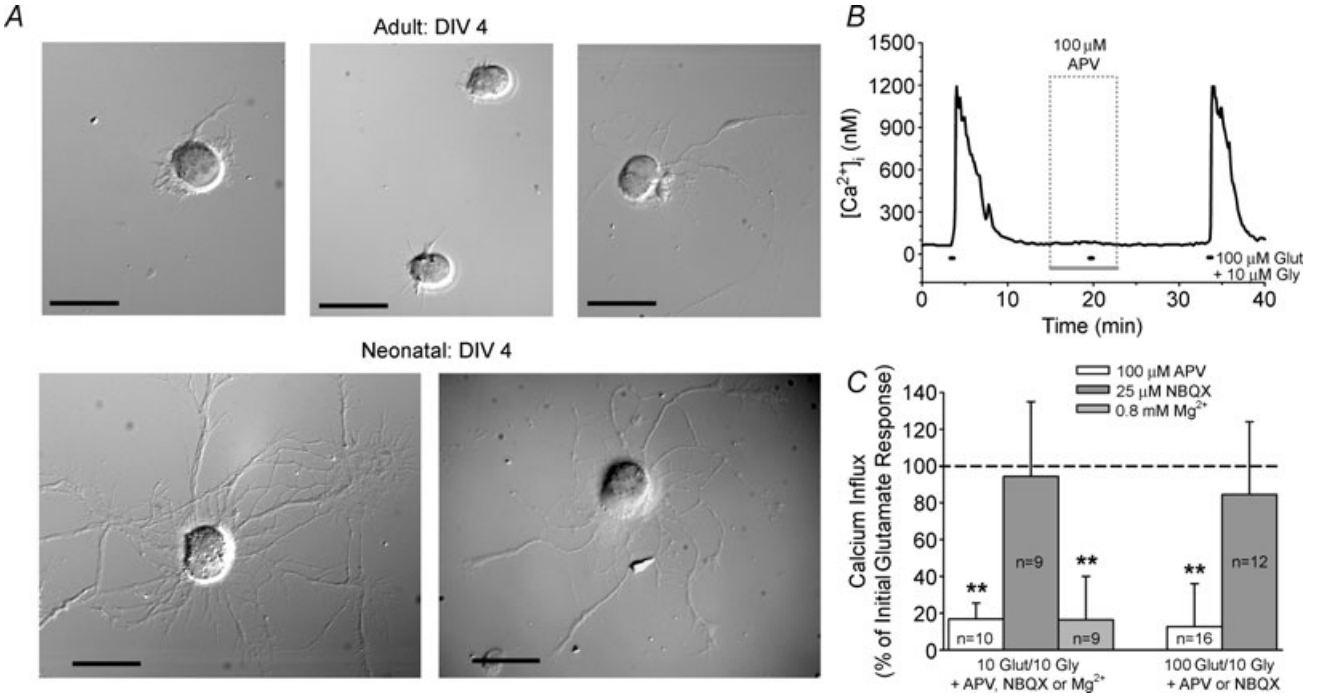

Figure 6. Glutamate-induced Ca^{2+} influx in immunopanned RGCs generated from adult rats
A, DIC images of RGCs isolated from adult (6 weeks old) and neonatal (8 days old) rats after 4 days *in vitro* (DIV). In contrast to neonatal RGCs, adult RGCs exhibited little to no neurite outgrowth even after 4 days in culture. Scale bars = 25 μm. *B*, representative trace illustrating effect of NMDA-R antagonist APV on adult RGC responses to 100 μM glutamate (with 10 μM glycine; extracellular Mg^{2+} absent). *C*, mean data (change in $[Ca^{2+}]_i$ +1 S.D.) showing effect of glutamate receptor antagonists and extracellular Mg^{2+} on Ca^{2+} responses evoked by 10 and 100 μM glutamate in RGCs isolated from adult rats (normalized to initial response; dashed line). $^{**}P < 0.01$, Friedman ANOVA, Tukey, compared to initial and recovery responses.

removes glutamate, but not NMDA or kainate, from the extracellular milieu. At 500 μM, glutamate did elicit a detectable Ca^{2+} signal when coapplied with the glutamate transporter inhibitor TBOA (Fig. 7*B* and *C*). In Mg^{2+}-free conditions, the RGC responses to glutamate plus TBOA were significantly ($P < 0.01$, Friedman ANOVA, Tukey) reduced by APV but not ($P > 0.05$) by NBQX (Fig. 7*B* and *C*). Upon perfusion of the retinas with 0.8 mM

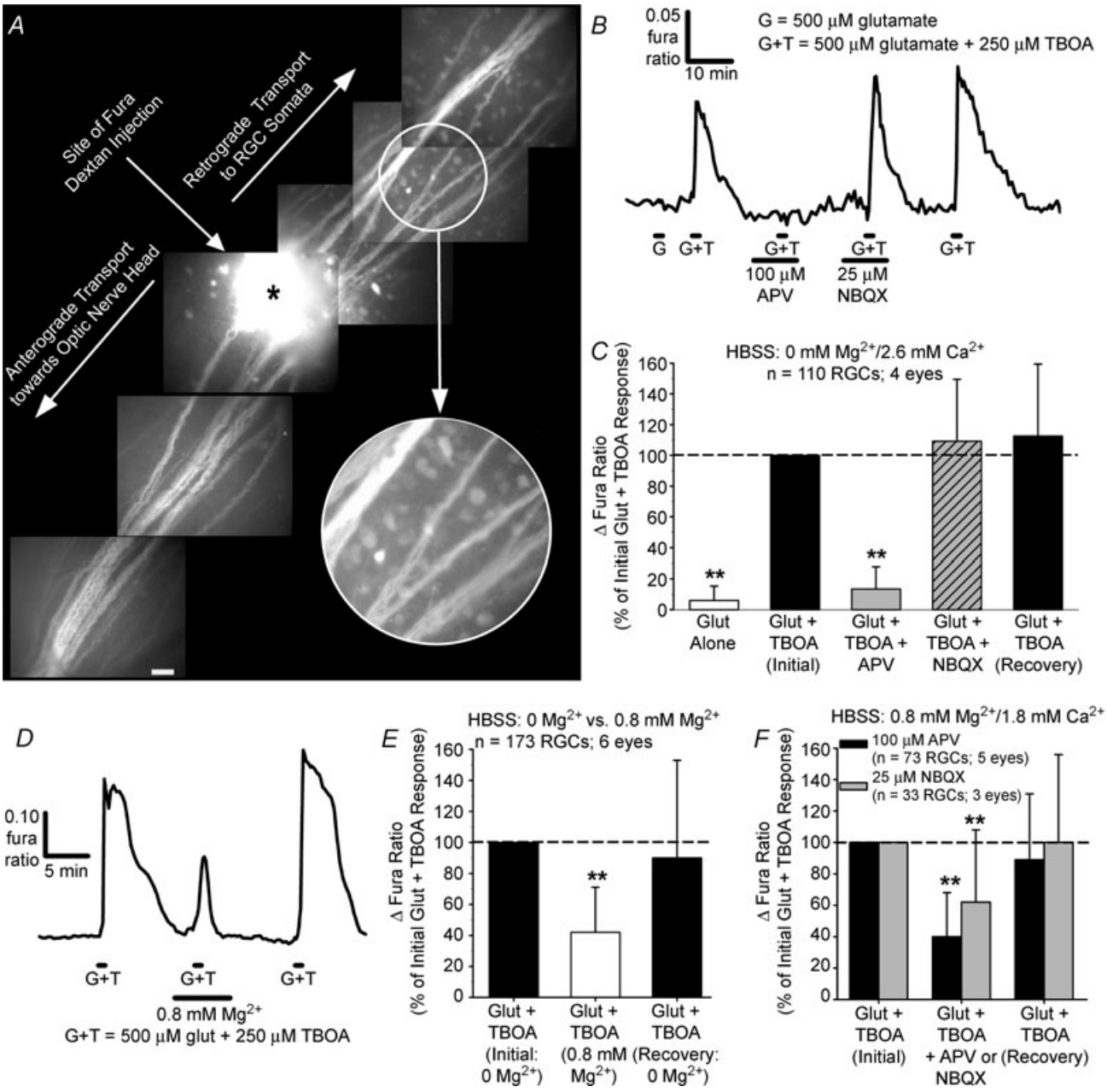

Figure 7. Glutamatergic Ca^{2+} dynamics of RGCs in adult rat retinal wholemounts
A, montage of fluorescence micrographs (380 nm excitation, 510 emission) showing retrograde loading of RGC somata following injection of fura dextran into the retinal wholemount at the site denoted by an asterisk. Scale bar = 50 μm. The encircled area is shown at higher magnification to highlight individual dye-loaded RGC somata. *B*, representative trace illustrating that glutamate is more effective at evoking a detectable Ca^{2+} signal when coapplied with the glutamate transporter inhibitor TBOA, and the glutamate plus TBOA response is blocked by APV but not affected by NBQX with extracellular Mg^{2+} absent. *C*, mean normalized data (Δfura ratio +1 S.D.) summarizing effect of glutamate receptor antagonists on RGC responses in Mg^{2+}-free conditions. *D* and *E*, example trace (*D*) and mean normalized data (*E*) showing inhibitory effect of extracellular Mg^{2+} (0.8 mM) on RGC responses to glutamate plus TBOA in this intact retina preparation. *F*, mean normalized data summarizing effect of glutamate receptor antagonists on glutamatergic RGC responses with 0.8 mM extracellular Mg^{2+} present. $^{**}P < 0.01$, Friedman ANOVA, Tukey, compared to initial and recovery responses to glutamate plus TBOA.

Mg^{2+}, RGC Ca^{2+} responses were again smaller ($P < 0.01$) relative to the responses elicited from the same RGCs with extracellular Mg^{2+} absent (Fig. 7*D* and *E*). With 0.8 mM Mg^{2+} present in the external solution, the RGC Ca^{2+} responses evoked by glutamate plus TBOA were significantly ($P < 0.01$) inhibited by either APV and NBQX (Fig. 7*F*). Therefore, as in isolated RGCs, NMDA-Rs had a predominant role in mediating the glutamate-induced rise in RGC Ca^{2+} levels in this intact retina preparation in Mg^{2+}-free conditions, while the activation of both NMDA-Rs and AMPA/kainate-Rs facilitates RGC Ca^{2+} responses with extracellular Mg^{2+} present (see Discussion for further explanation).

RGC calcium dynamics and deregulation during prolonged glutamate exposure

RGC Ca^{2+} dynamics were next monitored during a more prolonged glutamate exposure of 1 h. For these experiments, immunopanned RGCs from neonatal rats were again used, and all experiments were performed in Mg^{2+}-free HBSS unless otherwise specified. In other central neurons, it has been reported that the high affinity Ca^{2+} indicator fura-2 can underestimate the rise in $[Ca^{2+}]_i$ associated with glutamate excitotoxicity due to dye saturation (Hyrc *et al.* 1997; Stout & Reynolds, 1999). To minimize this possibility, the low-affinity Ca^{2+} indicator dye fura-4F (K_D ~770 nM) was instead employed. The overall design of these experiments is illustrated in Fig. 8. The fura-4F ratio was monitored in RGCs treated for 1 h with different concentrations of glutamate plus 10 μM glycine. Upon glutamate exposure, RGCs generally exhibited an abrupt rise in the fura-4F ratio, which was then maintained at a relatively stable level (Fig. 8*C*). Cells that maintained this $[Ca^{2+}]_i$ homeostasis throughout the 1 h exposure showed recovery towards baseline levels during the ensuing 15 min wash-out period. However, certain cells exhibited a latent loss in Ca^{2+} homeostasis that was characterized by a large and irreversible rise in the fura-4F ratio. Cells that underwent this delayed Ca^{2+} deregulation (DCD), previously described in other central neurons (Manev *et al.* 1989; Randall & Thayer, 1992; Tymianski *et al.* 1993; Rajdev & Reynolds, 1994), showed no recovery during the wash-out period, with the fura-4F ratio remaining elevated (Fig. 8*E*). Calibration of fura-4F ratios to $[Ca^{2+}]_i$ was not performed because the irreversible rise in $[Ca^{2+}]_i$ that occurred during DCD exceeded the dynamic range of the fura-4F indicator dye.

At the end of some of these experiments, the cells were incubated with fluorescently tagged annexin V that had been added to the microscope chamber. During apoptosis, the lipid phosphatidylserine is translocated from the cytoplasmic side of the plasma membrane to its outer surface (Koopman *et al.* 1994), and therefore annexin V fluorescence can be used to identify apoptotic cells. Necrotic cells can also be stained by annexin V, as this marker can enter lysed cells and stain phosphatidylserine on the inner membrane surface. Annexin V fluorescence was therefore used as a general marker for cell death, rather than to distinguish apoptosis from necrosis. As evident in Fig. 8*F*, the three cells that underwent Ca^{2+} deregulation (denoted by numbers 5, 9 and 12) were stained by annexin V at the conclusion of the experiment.

To be consistent with the studies employing 30 s glutamate treatments (Figs 1–5), the effect of a 1 h exposure to glutamate in the presence and absence of glutamate receptor blockers (Figs 9 and 10) was tested on RGCs that had been cultured for 1–3 days. Cells from short-term cultures were chosen for experiments throughout this work because the purified RGCs are likely to receive much less glutamatergic stimulation in culture as compared to *in vivo*, and it was not known whether glutamate receptor expression and/or Ca^{2+} buffering is consequently altered in RGCs during long-term culture. However, a concern with the use of semiacute cultures is that RGCs that had been injured during the dissociation process may not have yet been completely eliminated from the cultures. The Ca^{2+} imaging technique provided two separate measures of cell viability to preclude unhealthy cells from influencing the results regarding the neurotoxicity of glutamate. First, similar to the commonly used cell viability marker calcein AM, the fura dye contains an AM ester that must be enzymatically cleaved by endogenous esterases in order for cells to exhibit fura fluorescence. Thus, unviable cells could not be imaged and were automatically excluded from these experiments (see two example annexin V-positive cells, denoted by arrows in Fig. 8*A*, *B* and *D*–*F*, which showed negligible fura fluorescence). Second, RGCs that exhibited elevated baseline fura ratios (such as annexin V-positive cell 4 in Fig. 8*A*, *B* and *D*–*F*, denoted by green trace in Fig. 8*C*) were deemed unhealthy and excluded from analysis (a criterion of baseline fura-4F ratio > 0.3 was used to exclude cells). Furthermore, to determine whether DCD occurrence was unique to acute RGC cultures, a group of RGCs ($n = 34$) that had been cultured for 7 days were treated with 100 μM glutamate for 1 h. DCD was observed in 14.7% (5 of 34) of these RGCs (see example in Fig. 8*G*), confirming that this phenomenon also occurs in RGCs cultured for 1 week. The morphological changes exhibited by a representative DIV 7 RGC undergoing excitotoxic death is illustrated in Fig. 8*H* and in Supplemental Movie 1.

For the data shown in Figs 9 and 10, all results are based on the pooled data from at least three different immunopanned RGC cultures. Ca^{2+} influx in these experiments was calculated as the Δfura-4F ratio, the peak ratio during the first 400 s of glutamate exposure minus the mean baseline ratio before glutamate treatment. The time frame of 400 s was utilized in order to compare the Ca^{2+} levels,

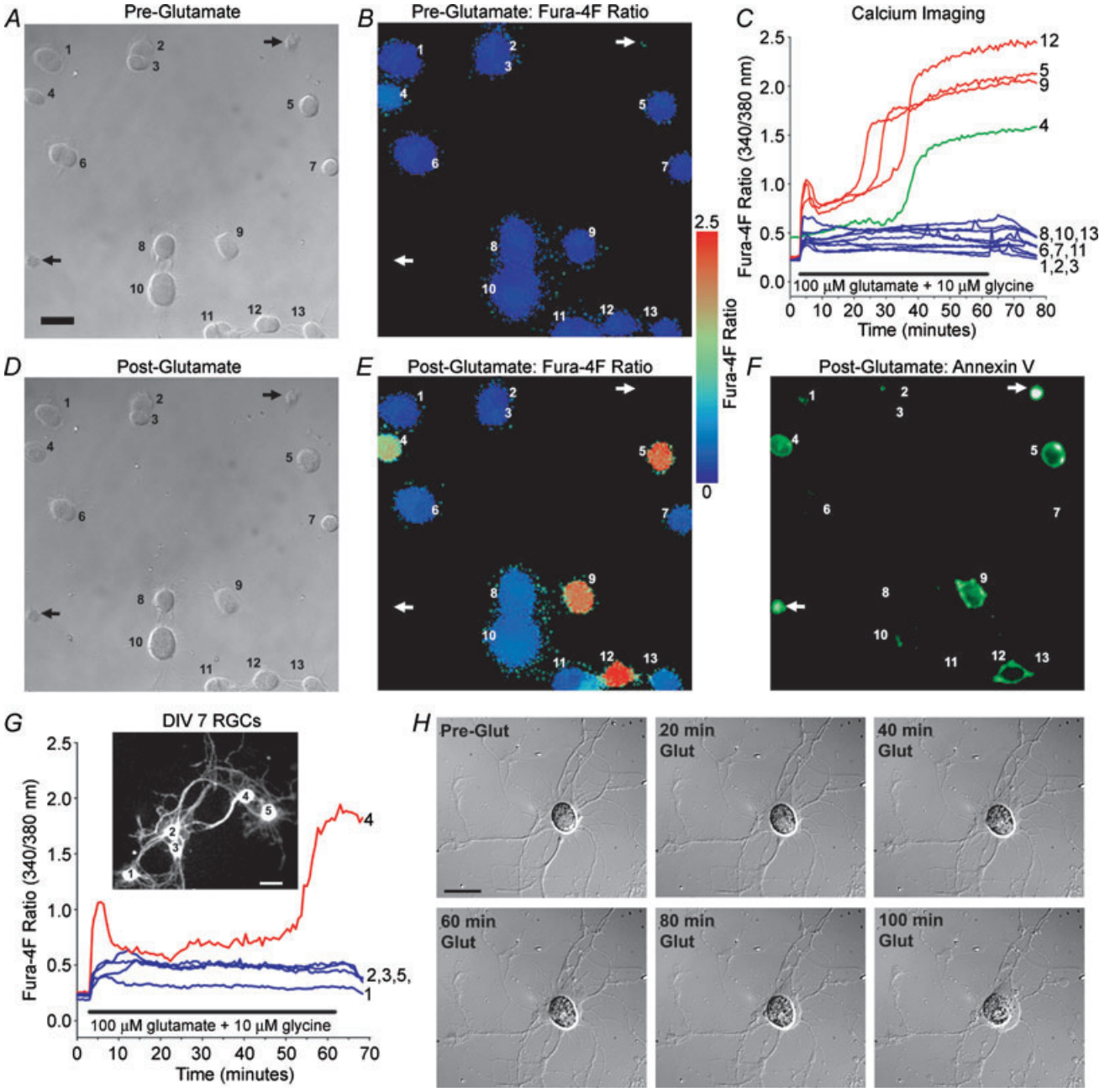

Figure 8. Excitotoxic death of isolated RGCs is associated with delayed calcium deregulation (DCD)
A and *B*, DIC image (*A*) and pseudocolour image (*B*) of the fura-4F ratio (340/380 nm) of example RGCs, isolated from neonatal rats (first day *in vitro* [DIV]), prior to glutamate exposure. *C*, the fura-4F ratio was monitored in these RGCs while they were continuously superfused with 1000 μM glutamate (plus 10 μM glycine; in Mg^{2+}-free HBSS) for 1 h, followed by 15 min wash-out. Of the 13 RGCs imaged, 9 cells maintained homeostatic Ca^{2+} levels throughout glutamate treatment and recovered towards baseline levels during wash-out (blue traces). DCD was evident in 3 cells (denoted by numbers 5, 9 and 12), and was characterized by a large increase in the fura ratio with no recovery (red traces). RGCs with elevated baseline fura ratios (> 0.3), such as cell 4 (green trace), were excluded from analysis. *D–F*, DIC image (*D*), pseudocolour image of the fura-4F ratio (*E*) and annexin V fluorescence (*F*) in these same cells after glutamate exposure and wash-out. The DCD-exhibiting RGCs (cells 5, 9 and 12) and the RGC with elevated baseline $[Ca^{2+}]_i$ (cell 4) were stained by the death marker annexin V. Note that the cells denoted by the arrows also were annexin V-positive, but these unviable cells did not load the fura dye (absent from ratiometric images). *G*, fura-4F ratio traces for five RGCs on DIV 7 that were treated with 100 μM glutamate (plus 10 μM glycine; in Mg^{2+}-free HBSS) for 1 h. Inset: fura fluorescence image (380 nm excitation) of the corresponding five RGCs from which the fura traces were recorded, with enhanced contrast for neurite visualization. *H*, DIC images of a glutamate-treated RGC (DIV 7), illustrating the morphological changes that occur in an RGC undergoing excitotoxic death (see Supplemental Movie 1).

prior to the onset of DCD, of those cells that deregulated *versus* those that did not (no cells underwent deregulation during the first 400 s). Also, the peak fura ratio (not including the increase associated with DCD) generally occurred during this initial response before decaying to a stable level. There was no significant difference in the mean initial Ca^{2+} influx between cells treated with either 100 μM or 1000 μM glutamate, while the influx induced by 10 μM glutamate was slightly less ($P < 0.05$, $Q = 3.001$, Kruskal–Wallis ANOVA, Dunn's) than that for 100 μM (Fig. 9*A*). These results are consistent with the findings in Fig. 1 that showed that 100 μM glutamate was sufficient to evoke maximum Ca^{2+} responses in isolated RGCs, and verifies that the earlier findings were not due to saturation of the high-affinity fura-2 dye. DCD occurred in 18–28% of the RGCs exposed to 10, 100 and 1000 μM glutamate for 1 h (Fig. 9*B*), and there was no significant difference ($P = 0.351$, Chi-square) in the proportion of cells undergoing DCD during treatment with the different glutamate concentrations. As a control, DCD was not observed in any RGCs ($n = 41$) that were maintained in HBSS (no glutamate) for 1 h.

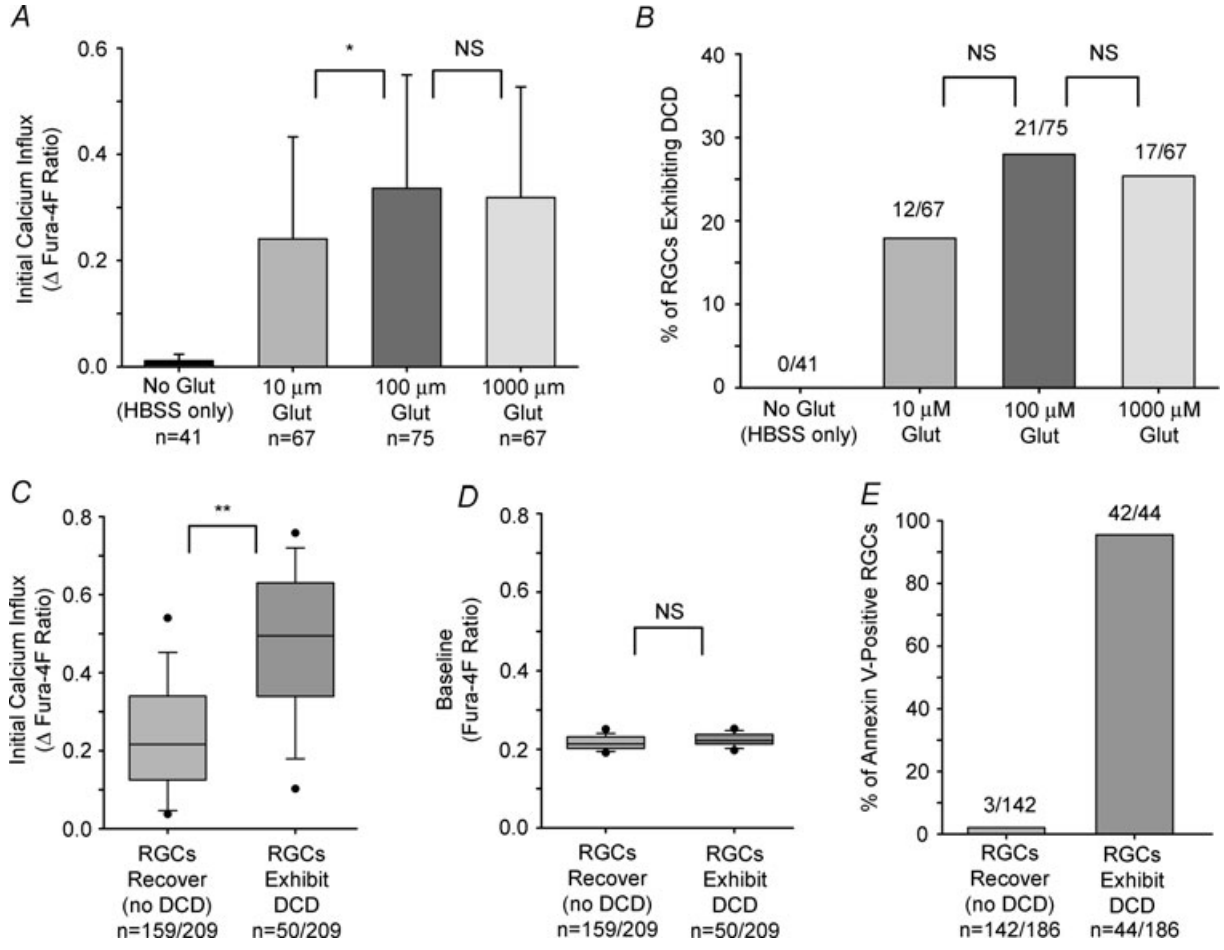

Figure 9. Relationship of glutamate concentration and Ca^{2+} influx to DCD incidence in isolated RGCs
A, mean Ca^{2+} influx (peak fura-4F ratio over first 400 s of glutamate exposure minus baseline ratio; +1 S.D.) induced by 10, 100 and 1000 μM glutamate (plus 10 μM glycine; in Mg^{2+}-free HBSS) during the 1 h glutamate exposure. *B*, the proportion of cells exhibiting DCD in each treatment group. A group of RGCs were maintained in HBSS for 1 h (glutamate absent) as controls. *C* and *D*, box-plots of pooled data for all RGCs treated with glutamate (10–1000 μM; $n = 209$) illustrating that Ca^{2+} responses were significantly related to initial Ca^{2+} influx (*C*), but not to baseline Ca^{2+} levels (*D*). The upper and lower boundaries of the box indicate the 75th and 25th percentiles, the line within the box marks the median, the whiskers above and below the box indicate the 90th and 10th percentiles, while the points represent outlying data. *E*, of the 209 RGCs treated with glutamate, 186 of these RGCs were examined for annexin V fluorescence at the conclusion of the experiment. Annexin V staining paralleled the imaging data, confirming that DCD was associated with cellular death. $^*P < 0.05$, $^{**}P < 0.01$, Kruskal–Wallis ANOVA, Dunn's *post hoc* test for Ca^{2+} influx data (comparing the three glutamate-treated groups); Chi-square for DCD incidence data (comparing the three glutamate-treated groups); Mann–Whitney test for comparison of box-plot data.

Pooling the data together for the three glutamate concentrations, the incidence of DCD was related to the magnitude of the glutamate-induced Ca^{2+} responses, as RGCs with larger Ca^{2+} responses were most likely to deregulate (Fig. 9*C*). This susceptibility was not linked to baseline Ca^{2+} levels (Fig. 9*D*), indicating that DCD-exhibiting cells were not already injured prior to glutamate exposure. The presence of annexin V fluorescence was determined at the conclusion of the experiment for 186 of the RGCs treated with glutamate (Fig. 9*E*). The vast majority of deregulating RGCs in this group were stained by annexin V (42 of 44 cells), while RGCs that recovered from glutamate treatment usually did not exhibit annexin V fluorescence (139 of 142 cells were annexin V-negative). Therefore, these results indicate that the RGCs that underwent DCD were indeed dead or dying.

To assess the effect of glutamate receptor inhibition on DCD occurrence, RGCs were exposed for 1 h to 100 μM glutamate (plus 10 μM glycine; in Mg^{2+}-free HBSS unless noted otherwise) with AMPA/kainate-R and NMDA-R blockers present. Each of the tested

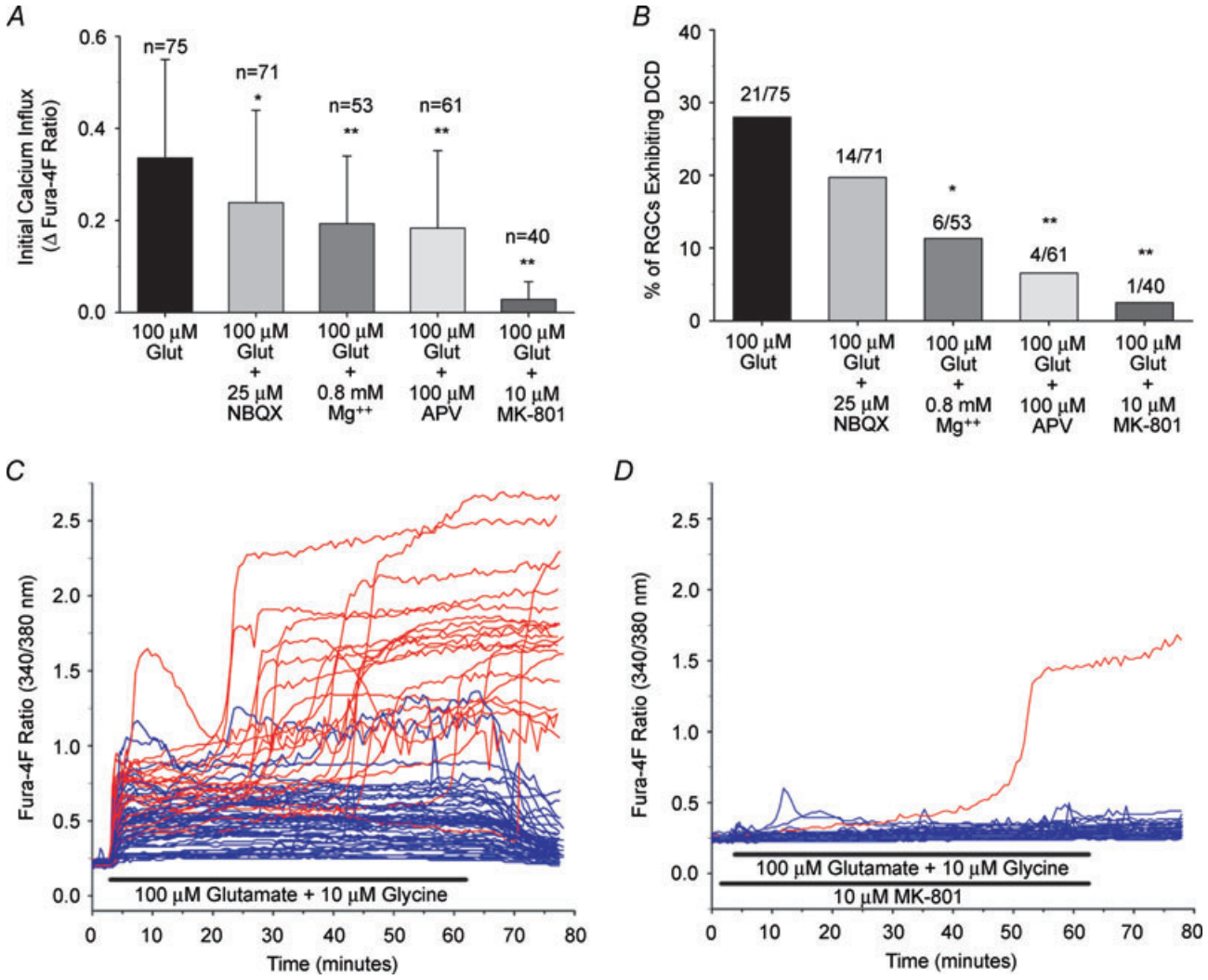

Figure 10. Effect of glutamate receptor blockade on Ca^{2+} influx and DCD occurrence in isolated RGCs
A, mean Ca^{2+} influx (peak fura-4F ratio over first 400 s of glutamate exposure minus baseline ratio; +1 S.D.) induced by 100 μM glutamate (plus 10 μM glycine) in the presence or absence of AMPA/kainate-R (NBQX) and NMDA-R (Mg^{2+}, APV and MK-801) blockers. The data for 100 μM glutamate (blockers absent) is re-plotted from data shown in Fig. 9. *B*, the proportion of cells exhibiting DCD in each treatment group. *C* and *D*, fura-4F ratio traces of all RGCs ($n = 75$) treated with 100 μM glutamate plus 10 μM glycine for 1 h (with 15 min wash-out) alone (*C*), and in the presence of the non-competitive NMDA-R antagonist MK-801 ($n = 40$) (*D*). RGCs exhibiting DCD are denoted by red traces while RGCs surviving the glutamate insult are denoted by blue traces. $^{*}P < 0.05$, $^{**}P < 0.01$, as compared to 100 μM glutamate-treated group; Kruskal–Wallis ANOVA, Dunn's *post hoc* test for Ca^{2+} influx data; Chi-square for DCD incidence data.

agents, NBQX (25 μM; AMPA/kainate-R antagonist), extracellular Mg^{2+} (0.8 mM; NMDA-R channel blocker), APV (100 μM; NMDA-R antagonist) and MK-801 (10 μM; NMDA-R antagonist), significantly ($P < 0.05$, Kruskal–Wallis ANOVA, as compared to group treated only with 100 μM glutamate) reduced the initial Ca^{2+} influx (Fig. 10*A*). RGCs treated with compounds targeting NMDA-Rs exhibited a significant reduction ($P < 0.01$, Chi-square, as compared to group treated with 100 μM glutamate alone) in DCD occurrence (Fig. 10*B*). Consistent with the observed relationship of calcium influx to DCD incidence (Fig. 9*C*), there was a general trend suggesting that greater reductions in glutamate-induced calcium influx were associated with fewer cells exhibiting DCD. APV (100 μM) was not as effective at blocking glutamate-induced Ca^{2+} signals as in the brief (30 s) glutamate pulse experiments (see Fig. 3), but this is likely to be because APV is a competitive antagonist and competes with glutamate throughout the 1 h exposure period. The non-competitive antagonist MK-801 provided near-complete protection, and its effect on glutamate-induced Ca^{2+} influx and DCD incidence is perhaps best illustrated by examining the optical recordings for all RGCs ($n = 40$) treated with 100 μM glutamate in the presence of MK-801 (Fig. 10*D*) as compared to traces for RGCs ($n = 75$) treated with 100 μM glutamate alone (Fig. 10*C*). In agreement with the previous experiments employing 30 s glutamate treatments (Fig. 3), blockade of NMDA-Rs with MK-801 nearly abolished Ca^{2+} influx, and significantly prevented the incidence of Ca^{2+} deregulation and ensuing cell death.

Discussion

In this work, we showed that RGC excitotoxicity was characterized by delayed Ca^{2+} deregulation, and that RGCs exhibiting larger glutamate-evoked Ca^{2+} responses were more likely to undergo DCD. Glutamate-induced Ca^{2+} influx occurred predominantly through NMDA-R activation in RGCs isolated from neonatal or adult rats and in RGCs from retinal wholemounts. Antagonism of NMDA-Rs significantly reduced the occurrence of DCD and protected RGCs from excitotoxic death.

Glutamate-induced RGC calcium influx is mediated primarily by NMDA-Rs

An increase in RGC $[Ca^{2+}]_i$ occurred following stimulation of either NMDA-Rs or AMPA/kainate-Rs with their respective selective agonists, NMDA and kainate, confirming that glutamate could potentially alter RGC Ca^{2+} dynamics through either pathway. In Mg^{2+}-free external solution, the NMDA-R antagonist APV abolished Ca^{2+} responses induced by a low glutamate concentration (10 μM) in RGCs isolated from neonatal rats, and blocked the majority of that due to a saturating glutamate concentration (100 μM). The AMPA/kainate-R antagonist NBQX had a small but significant effect on only RGC responses to 100 μM glutamate. As compared to NMDA-Rs, AMPA/kainate-Rs have a lower affinity for glutamate and desensitize quickly (Dingledine *et al.* 1999). These characteristics offer a mechanistic explanation for the findings of the present study: at near-threshold glutamate concentrations, AMPA/kainate-Rs are not stimulated and the response is entirely NMDA-R-mediated; at higher glutamate concentrations, AMPA/kainate-Rs are activated but desensitize quickly and contribute only a minor portion of the overall Ca^{2+} signal.

Consistent with a role for NMDA-Rs, the changes in RGC $[Ca^{2+}]_i$ produced by the glutamate treatments were reduced by the addition of Mg^{2+} to the superfusing solution and they were potentiated with the coapplication of glycine. With extracellular Mg^{2+} present, a similar reduction in the glutamate-induced Ca^{2+} responses was observed following antagonism of either NMDA-Rs or AMPA/kainate-Rs (using MK-801 and NBQX, respectively). Thus, while the effect of NMDA-R blockade on RGC glutamate responses was comparable regardless of external Mg^{2+} levels, the inhibitory effect of NBQX was more pronounced when the bathing solution contained Mg^{2+}. The most parsimonious explanation for these data is that AMPA/kainate-R activation is primarily required to depolarize RGCs and relieve the NMDA-R Mg^{2+}-block, rather than directly contributing to the rise in $[Ca^{2+}]_i$. Therefore, stimulation of both NMDA-Rs and AMPA/kainate-Rs is necessary for robust glutamate-related RGC Ca^{2+} responses with external Mg^{2+} present but, as shown by the experiments with extracellular Mg^{2+} absent, the Ca^{2+} signal itself is mostly mediated through NMDA-R activation.

Ca^{2+} can flow directly through glutamate receptor-associated channels or through VGCCs following neuronal depolarization. By blocking L- and N-type (Ca_V1 and $Ca_V2.2$) VGCCs, we found that influx through these channels contributes one-third, on average, of the RGC Ca^{2+} signal due to a saturating (100 μM) concentration of glutamate. In contrast, the Ca^{2+} responses induced by 10 μM glutamate were not significantly affected by the VGCC blocking cocktail, suggesting that the Ca^{2+} signals evoked by this concentration of glutamate (shown to be near-threshold under our recording conditions) were predominantly mediated by direct flux through NMDA-R channels. It is possible that VGCC involvement was underestimated, as only L- and N-type VGCCs were targeted, but these channels have been shown to mediate the majority of the Ca^{2+} current in rat RGCs (Karschin &

Lipton, 1989; Schmid & Guenther, 1999). In addition, while the average magnitude of the RGC Ca^{2+} responses to 200 μM NMDA was not statistically different from the responses evoked by 200 μM kainate, the VGCC blockers significantly affected the kainate-driven but not the NMDA-driven Ca^{2+} signals. These results imply that at this concentration, NMDA stimulates considerable Ca^{2+} flux through NMDA-R channels without depolarizing the neuron to the threshold potential for VGCC activation. Although our data do not rule out a contribution for Ca^{2+}-permeable AMPA/kainate-Rs, they do indicate that 200 μM kainate depolarized the RGCs more than 200 μM NMDA (presumably due to proportionally greater inward current through AMPA/kainate-R channels) and that VGCC-mediated Ca^{2+} flux comprises a significant component of the kainate-induced Ca^{2+} responses of the isolated RGCs.

A potential concern in using RGC cultures is that dissociation alters the glutamate receptor expression from that *in vivo*. There is evidence, based on electrophysiological recordings and immunohistochemical analysis, that AMPA/kainate-Rs reside within synaptic clefts while NMDA-Rs on rat RGCs are instead located extrasynaptically (Chen & Diamond, 2002; Zhang & Diamond, 2006), although other work has suggested that extrasynaptic NMDA-Rs are a feature of ON RGCs rather than OFF RGCs (Sagdullaev *et al.* 2006). As RGCs in purified cultures develop few synapses (Ullian *et al.* 2001), AMPA/kainate-Rs may be underrepresented in immunopanned RGCs. Ca^{2+} imaging of RGCs in retinal wholemounts addressed this issue. Consistent with previous work demonstrating the efficiency of glutamate uptake in this intact retina preparation (Hartwick *et al.* 2005), 500 μM glutamate alone had no effect on RGCs but it induced a detectable Ca^{2+} signal with the coapplication of the glutamate transporter inhibitor TBOA. The bath application of glutamate plus TBOA is meant to mimic the rise in extracellular glutamate levels that occurs when glutamate transporter function is disrupted in conditions such as ischaemia/hypoxia (for review, see Camacho & Massieu, 2006). Under Mg^{2+}-free conditions, the RGC responses to glutamate plus TBOA were blocked by NMDA-R but not AMPA/kainate-R antagonism, in agreement with the results obtained using the cultured RGCs. With extracellular Mg^{2+} present, the glutamate-related Ca^{2+} signals were reduced and there was increased inhibition of the responses by NBQX, findings that were again similar to those observed using immunopanned RGCs from neonatal rats. These data, along with comparable data obtained from isolated RGCs panned from adult rat retinas, argue against developmental differences in the mechanisms underlying glutamatergic Ca^{2+} dynamics in 7- to 8-day-old rats relative to those in adult rats.

RGC excitotoxicity is accompanied by delayed calcium deregulation

During prolonged exposure (1 h) to glutamate (10–1000 μM), approximately one-quarter (18–28%) of the immunopanned RGCs exhibited a latent loss of calcium homeostasis. This phenomenon, termed DCD, has been described in a number of other central neurons, including cerebellar granule (Manev *et al.* 1989), hippocampal (Randall & Thayer, 1992), spinal (Tymianski *et al.* 1993) and cortical (Rajdev & Reynolds, 1994) neurons, but this work represents its first characterization in a retinal neuron. RGCs undergoing DCD did not exhibit any recovery during the 15 min wash-out period, while RGCs that maintained a plateau $[Ca^{2+}]_i$ throughout glutamate treatment recovered towards baseline levels. As there was no significant difference in the baseline fura-4F ratios between RGCs that developed DCD and those that did not, and RGCs that were maintained in only HBSS (no glutamate added) did not exhibit DCD, it is highly unlikely that the occurrence of DCD and subsequent cell death was not directly related to glutamate treatment. Annexin V staining at the culmination of the imaging experiments resulted in essentially exclusive labelling of RGCs that had underwent DCD, consistent with previous work showing DCD precedes, or at least coincides with, excitotoxic neuronal death (Tymianski *et al.* 1993).

Interestingly, the number of RGCs exhibiting a latent loss of Ca^{2+} homeostasis during the prolonged glutamate exposure was not appreciably different for the three glutamate concentrations (10, 100, 1000 μM) tested. Even at 1000 μM, only about one-quarter of the RGCs deregulated after 1 h, showing a similar steady loss of cells as the 1 h treatment with 10 or 100 μM glutamate. This finding suggests that it is extended exposure periods, and not brief contact with high concentrations, that triggers glutamate's toxic effects on RGCs. By inhibiting NMDA-R activation with either Mg^{2+}, the competitive antagonist APV or the non-competitive antagonist MK-801, RGC Ca^{2+} responses were reduced and the occurrence of DCD significantly decreased. The AMPA/kainate-R antagonist NBQX had a small effect on RGC Ca^{2+} responses, but its effect in preventing DCD was not statistically significant. Therefore, NMDA-R activation played a major role in DCD and glutamate-related RGC death.

The nature of the secondary $[Ca^{2+}]_i$ increase during DCD in RGCs was not assessed in the current work and represents a topic for future study. The mechanisms underlying DCD in other central neurons have been reported to involve either a reduction in the functional capacity of Ca^{2+} efflux mechanisms or a latent activation of plasma membrane ion channels (or a combination of both scenarios; for review, see Chinopoulos & Adam-Vizi, 2006). In support of reduced Ca^{2+} efflux, it has been demonstrated that glutamate-induced DCD in cerebellar

granule neurons involves the calpain-mediated proteolysis of Na^+/Ca^{2+} exchangers, which renders the neurons incapable of extruding Ca^{2+} in sufficient amounts to maintain homeostasis (Bano *et al.* 2005). In agreement with the secondary Ca^{2+} influx hypothesis, there is other evidence that excitotoxicity-related DCD in hippocampal and cortical neurons is due to the activation of a Ca^{2+}-permeable channel that can be blocked by gadolinium, lanthanum or 2-aminoethoxydiphenyl borate (Chinopoulos *et al.* 2004; Deshpande *et al.* 2007). The identity of this putative channel remains unknown, but traditionally studied Ca^{2+}-permeable channels such as glutamate receptors and VGCCs have been ruled out (Manev *et al.* 1989; Randall & Thayer, 1992; Deshpande *et al.* 2007).

There was considerable interneuronal variability in the magnitude of the glutamate-evoked Ca^{2+} signals in immunopanned RGCs, and this variability was evident with either the 30 s or 1 h glutamate treatment protocols (and with the use of either fura-2 or fura-4F indicator dyes). While the dissociation procedure may have contributed to this variability, studies assessing the accumulation of the cation channel permeant agmatine in mammalian retinas exposed to glutamatergic agonists indicate that RGCs are indeed a heterogeneous group of neurons with a broad spectrum of responses to excitatory input (Marc, 1999*a*,*b*; Marc & Jones, 2002; Sun *et al.* 2003). Furthermore, single-cell PCR analysis of mouse RGCs indicates that, while virtually all of these neurons express AMPA-, kainate- and NMDA-Rs, there is considerable intercell variability in the expression of the different subunits for these glutamate receptors (Jakobs *et al.* 2007), thereby providing a potential molecular basis for the heterogeneity of the glutamatergic Ca^{2+} responses. The magnitude of an individual RGC's glutamate-induced Ca^{2+} signal was linked to its susceptibility to excitotoxicity, as RGCs that displayed larger Ca^{2+} responses were more likely to undergo DCD. This finding is in general agreement with the 'Ca^{2+} load' hypothesis, which suggests that excitotoxic neuronal death correlates with the rise in $[Ca^{2+}]_i$ (Hartley *et al.* 1993; Eimerl & Schramm, 1994; Lu *et al.* 1996). A competing, yet not mutually exclusive, proposal is that the route of Ca^{2+} entry ('source specificity' hypothesis) is a greater death determinant than the overall $[Ca^{2+}]_i$ change, with Ca^{2+} influx through NMDA-Rs being more lethal than influx through VGCCs or AMPA/kainate-Rs (Tymianski *et al.* 1993; Sattler *et al.* 1998). As NMDA-Rs were the major contributor to RGC Ca^{2+} responses, blocking NMDA-R activation dramatically reduced Ca^{2+} influx and essentially eliminated the occurrence of DCD. Therefore, the results of these experiments are potentially compatible with either theory, and further research is necessary to test the 'Ca^{2+} load' *versus* 'source specificity' hypotheses in RGCs.

Many of the experiments in the current work were performed using a superfusing solution that contained no Mg^{2+}, an experimental paradigm that is consistent with previous studies that have investigated DCD in other central neurons (see below). With Mg^{2+} in the external bath, a rise in $[Ca^{2+}]_i$ could still be elicited from the isolated RGCs and the RGCs in the intact retina preparations, albeit to a lesser extent than when Mg^{2+} was absent. Similarly, the addition of Mg^{2+} to the extracellular milieu reduced, but did not completely protect against, the occurrence of DCD in the cultured RGCs. However, it is not necessarily a valid assumption that the experiments in Mg^{2+}-containing HBSS serve as a better indicator for RGC susceptibility to excitotoxicity in the living eye. While it is unlikely that Mg^{2+}-free conditions occur in the retina *in vivo*, the effectiveness of Mg^{2+} in blocking RGC NMDA-Rs is likely to be more pronounced in the purified cultures and the retinal wholemounts due to the voltage dependency of this inhibition. With synaptic glutamatergic input eliminated (the chromophore-regenerating retinal pigment epithelium was removed in the retinal wholemounts), the RGCs in these two *in vitro* preparations would be expected to be more hyperpolarized than RGCs *in vivo* and thus more affected by Mg^{2+}. The depolarization of RGCs due to AMPA/kainate-R activation, shown here to play a role in facilitating NMDA-R-mediated Ca^{2+} influx when Mg^{2+} is present, would be mediated *in vivo* through the recurrent bursts of synaptically released glutamate generated in retinal responses to visual stimuli. That RGC NMDA-R activation can occur under physiological conditions is supported by a number of studies that have shown that intravitreal injections of NMDA in live rodents results in RGC death (examples include Siliprandi *et al.* 1992; Lam *et al.* 1999; Schlamp *et al.* 2001; Manabe *et al.* 2005; Nakazawa *et al.* 2005; Pernet *et al.* 2007; Reichstein *et al.* 2007).

Based on experiments using RGCs in purified cultures and in retinal wholemounts, Ullian *et al.* (2004) reported that these retinal neurons are invulnerable to the excitotoxic actions of glutamate. Our data instead indicate that excitotoxic death can occur in at least a subpopulation of RGCs, and this death is associated with a similar dysregulation of $[Ca^{2+}]_i$ (DCD) that has been observed in other central neurons. The susceptibility of RGCs to excitotoxicity observed in our study is in agreement with the many *in vivo* studies of NMDA-R-mediated RGC death (examples listed in preceding paragraph). One reason for the differences in our findings may be related to the external solution used in the glutamate exposure experiments. In the present study, the immunopanned RGCs were transferred to HBSS for glutamate treatments, rather than adding glutamate to Neurobasal/B27 culture medium as in Ullian *et al.* (2004). Besides Mg^{2+}, this culture medium contains vitamins, minerals, and

antioxidants that are designed to enhance neuronal survival (Brewer *et al.* 1993). In particular, oxidative stress caused by free radical formation (such as peroxynitrate generated from nitric oxide) has been implicated as a downstream effector of NMDA-R-mediated excitotoxicity (Dawson *et al.* 1991; Dugan *et al.* 1995; Reynolds & Hastings, 1995). The antioxidants in Neurobasal/B27 have been shown to be neuroprotective in models of glutamate-induced neuronal death (Perry *et al.* 2004), indicating that this culture medium may confound studies of excitotoxicity.

While our results dispute the assertion that RGCs are completely immune to the excitotoxic effects of glutamate, Ullian *et al.* (2004) provided strong evidence that RGCs are much less vulnerable to excitotoxic death than retinal amacrine cells and hippocampal neurons. In the current study, the percentage of RGCs undergoing DCD ($< 30\%$) during the 1 h exposure to glutamate was considerably less than the approximate 60–85% rate of DCD occurrence that has been observed in cultures of spinal (Tymianski *et al.* 1993), cortical (Chinopoulos *et al.* 2004), and cerebellar granule (Bano *et al.* 2005) neurons using similar glutamate treatment protocols and Ca^{2+} imaging protocols (including the use of Mg^{2+}-free external solution). Why RGCs are less susceptible to glutamate excitotoxicity, as compared to other types of neurons, remains an important question. Interestingly, Ullian *et al.* (2004) found that RGCs exhibited significantly smaller NMDA-evoked currents relative to hippocampal neurons. It is possible that the total number of NMDA-Rs or the subunit composition of the expressed NMDA-Rs is different in RGCs, relative to more vulnerable neuronal types. For example, NMDA-Rs that contain NR2A or NR2B subunits, as compared to those with NR2C or NR2D, show a higher sensitivity to Mg^{2+} block (Kuner & Schoepfer, 1996), while NMDA-Rs containing the NR3A subunit exhibit reduced whole-cell currents and Ca^{2+} permeability (Dingledine *et al.* 1999). Each of these subunits has been identified on rodent RGCs (Sucher *et al.* 2003; Ullian *et al.* 2004; Jakobs *et al.* 2007) but the relative expression of different NMDA-R subunit combinations has yet to be clarified for RGCs. Alternatively, there are also data supporting the existence of endogenous neuroprotective mechanisms in RGCs that are activated downstream of NMDA-R-associated Ca^{2+} influx and that could serve to prevent DCD. An increase of $[Ca^{2+}]_i$ in salamander RGCs has been shown to disrupt the organization of actin filaments in the cell membrane, and this actin remodelling may serve as a feedback mechanism to decrease Ca^{2+} influx and protect RGCs from excitotoxicity by reducing the risk of Ca^{2+} overload (Cristofanilli & Akopian, 2006; Cristofanilli *et al.* 2007). Similarly, it has been demonstrated that an increase in the expression of calcium/calmodulin-dependent protein kinase (CaMKIIαB) is stimulated in rat RGCs following glutamate treatment, and this signalling pathway is part of an intrinsic survival response that protects RGCs from excitotoxic death (Fan *et al.* 2007).

It has been over 50 years since Lucas & Newhouse (1957) first documented the lethal effects of glutamate with the observation that excessive doses of this excitatory amino acid destroyed inner retinal neurons, including RGCs. Glutamate excitotoxicity has been implicated in the pathogenesis of a number of CNS neurodegenerative disorders (Choi, 1988; Lipton & Rosenberg, 1994), and in the RGC death that occurs during retinal ischaemia associated with central and branch retinal artery and vein occlusions (for review, see Osborne *et al.* 2004). The identification of mechanisms distinguishing the excitotoxic pathway from physiological glutamatergic signalling could aid in the development of effective yet safe neuroprotective therapies.

References

Aizenman E, Frosch MP & Lipton SA (1988). Responses mediated by excitatory amino acid receptors in solitary retinal ganglion cells from rat. *J Physiol* **396**, 75–91.

Ascher P & Nowak L (1988). The role of divalent cations in the N-methyl-D-aspartate responses of mouse central neurones in culture. *J Physiol* **399**, 247–266.

Baldridge WH (1996). Optical recordings of the effects of cholinergic ligands on neurons in the ganglion cell layer of mammalian retina. *J Neurosci* **16**, 5060–5072.

Bano D, Young KW, Guerin CJ, Lefeuve R, Rothwell NJ, Naldini L, Rizzuto R, Carafoli E & Nicotera P (2005). Cleavage of the plasma membrane Na^+/Ca^{2+} exchanger in excitotoxicity. *Cell* **120**, 275–285.

Bansal A, Singer JH, Hwang BJ, Xu W, Beaudet A & Feller MB (2000). Mice lacking specific nicotinic acetylcholine receptor subunits exhibit dramatically altered spontaneous activity patterns and reveal a limited role for retinal waves in forming ON and OFF circuits in the inner retina. *J Neurosci* **20**, 7672–7681.

Barres BA, Silverstein BE, Corey DP & Chun LL (1988). Immunological, morphological, and electrophysiological variation among retinal ganglion cells purified by panning. *Neuron* **1**, 791–803.

Boland LM, Morrill JA & Bean BP (1994). ω-Conotoxin block of N-type calcium channels in frog and rat sympathetic neurons. *J Neurosci* **14**, 5011–5027.

Brewer GJ, Torricelli JR, Evege EK & Price PJ (1993). Optimized survival of hippocampal neurons in B27-supplemented Neurobasal, a new serum-free medium combination. *J Neurosci Res* **35**, 567–576.

Camacho A & Massieu L (2006). Role of glutamate transporters in the clearance and release of glutamate during ischemia and its relation to neuronal death. *Arch Med Res* **37**, 11–18.

Chen S & Diamond JS (2002). Synaptically released glutamate activates extrasynaptic NMDA receptors on cells in the ganglion cell layer of rat retina. *J Neurosci* **22**, 2165–2173.

Chinopoulos C & Adam-Vizi V (2006). Calcium, mitochondria and oxidative stress in neuronal pathology. *FEBS J* **273**, 433–450.

Chinopoulos C, Gerencser AA, Doczi J, Fiskum G & Adam-Vizi V (2004). Inhibition of glutamate-induced delayed calcium deregulation by 2-APB and La^{3+} in cultured cortical neurones. *J Neurochem* **91**, 471–483.

Choi DW (1988). Glutamate neurotoxicity and diseases of the nervous system. *Neuron* **1**, 623–634.

Cristofanilli M & Akopian A (2006). Calcium channel and glutamate receptor activities regulate actin organization in salamander retinal neurons. *J Physiol* **575**, 543–554.

Cristofanilli M, Mizuno F & Akopian A (2007). Disruption of actin cytoskeleton causes internalization of $Ca_v1.2$ (α1D), L-type calcium channels in salamander retinal neurons. *Mol Vis* **13**, 1496–1507.

Dawson VL, Dawson TM, London ED, Bredt DS & Snyder SH (1991). Nitric oxide mediates glutamate neurotoxicity in primary cortical cultures. *Proc Natl Acad Sci U S A* **88**, 6368–6371.

Deshpande LS, Limbrick DD, Sombati S & DeLorenzo RJ (2007). Activation of a novel injury-induced calcium-permeable channel that plays a key role in causing extended neuronal depolarization and initiating neuronal death in excitotoxic neuronal injury. *J Pharmacol Exp Ther* **322**, 443–452.

Dingledine R, Borges K, Bowie D & Traynelis SF (1999). The glutamate receptor ion channels. *Pharmacol Rev* **51**, 7–61.

Dugan LL, Sensi SL, Canzoniero LM, Handran SD, Rothman SM, Lin TS, Goldberg MP & Choi DW (1995). Mitochondrial production of reactive oxygen species in cortical neurons following exposure to N-methyl-D-aspartate. *J Neurosci* **15**, 6377–6388.

Eimerl S & Schramm M (1994). The quantity of calcium that appears to induce neuronal death. *J Neurochem* **62**, 1223–1226.

Fan W, Li X & Cooper NG (2007). CaMKIIaB mediates a survival response in retinal ganglion cells subjected to a glutamate stimulus. *Invest Ophthalmol Vis Sci* **48**, 3854–3863.

Freedman SB, Dawson G, Villereal ML & Miller RJ (1984). Identification and characterization of voltage-sensitive calcium channels in neuronal clonal cell lines. *J Neurosci* **4**, 1453–1467.

Grynkiewicz G, Poenie M & Tsien RY (1985). A new generation of Ca^{2+} indicators with greatly improved fluorescence properties. *J Biol Chem* **260**, 3440–3450.

Guatteo E, Mercuri NB, Bernardi G & Knopfel T (1999). Group I metabotropic glutamate receptors mediate an inward current in rat substantia nigra dopamine neurons that is independent from calcium mobilization. *J Neurophysiol* **82**, 1974–1981.

Hama Y, Katsuki H, Tochikawa Y, Suminaka C, Kume T & Akaike A (2006). Contribution of endogenous glycine site NMDA agonists to excitotoxic retinal damage in vivo. *Neurosci Res* **56**, 279–285.

Hartley DM, Kurth MC, Bjerkness L, Weiss JH & Choi DW (1993). Glutamate receptor-induced $^{45}Ca^{2+}$ accumulation in cortical cell culture correlates with subsequent neuronal degeneration. *J Neurosci* **13**, 1993–2000.

Hartwick AT, Lalonde MR, Barnes S & Baldridge WH (2004). Adenosine A1-receptor modulation of glutamate-induced calcium influx in rat retinal ganglion cells. *Invest Ophthalmol Vis Sci* **45**, 3740–3748.

Hartwick AT, Zhang X, Chauhan BC & Baldridge WH (2005). Functional assessment of glutamate clearance mechanisms in a chronic rat glaucoma model using retinal ganglion cell calcium imaging. *J Neurochem* **94**, 794–807.

Hyrc K, Handran SD, Rothman SM & Goldberg MP (1997). Ionized intracellular calcium concentration predicts excitotoxic neuronal death: observations with low-affinity fluorescent calcium indicators. *J Neurosci* **17**, 6669–6677.

Ishida AT, Bindokas VP & Nuccitelli R (1991). Calcium ion levels in resting and depolarized goldfish retinal ganglion cell somata and growth cones. *J Neurophysiol* **65**, 968–979.

Jakobs TC, Ben Y & Masland RH (2007). Expression of mRNA for glutamate receptor subunits distinguishes the major classes of retinal neurons, but is less specific for individual cell types. *Mol Vis* **13**, 933–948.

Johnson JW & Ascher P (1987). Glycine potentiates the NMDA response in cultured mouse brain neurons. *Nature* **325**, 529–531.

Jonas P & Burnashev N (1995). Molecular mechanisms controlling calcium entry through AMPA-type glutamate receptor channels. *Neuron* **15**, 987–990.

Kao JP (1994). Practical aspects of measuring $[Ca^{2+}]$ with fluorescent indicators. *Methods Cell Biol* **40**, 155–181.

Karschin A & Lipton SA (1989). Calcium channels in solitary retinal ganglion cells from post-natal rat. *J Physiol* **418**, 379–396.

Khodorov B (2004). Glutamate-induced deregulation of calcium homeostasis and mitochondrial dysfunction in mammalian central neurones. *Prog Biophys Mol Biol* **86**, 279–351.

Koopman G, Reutelingsperger CP, Kuijten GA, Keehnen RM, Pals ST & van Oers MH (1994). Annexin V for flow cytometric detection of phosphatidylserine expression on B cells undergoing apoptosis. *Blood* **84**, 1415–1420.

Kuner T & Schoepfer R (1996). Multiple structural elements determine subunit specificity of Mg^{2+} block in NMDA receptor channels. *J Neurosci* **16**, 3549–3558.

Lam TT, Abler AS, Kwong JM & Tso MO (1999). N-methyl-D-aspartate (NMDA)-induced apoptosis in rat retina. *Invest Ophthalmol Vis Sci* **40**, 2391–2397.

Linden DJ, Smeyne M & Connor JA (1994). *Trans*-ACPD, a metabotropic receptor agonist, produces calcium mobilization and an inward current in cultured cerebellar Purkinje neurons. *J Neurophysiol* **71**, 1992–1998.

Lipton SA & Rosenberg PA (1994). Excitatory amino acids as a final common pathway for neurologic disorders. *N Engl J Med* **330**, 613–622.

Lu YM, Yin HZ, Chiang J & Weiss JH (1996). Ca^{2+}-permeable AMPA/kainate and NMDA channels: high rate of Ca^{2+} influx underlies potent induction of injury. *J Neurosci* **16**, 5457–5465.

Lucas DR & Newhouse JP (1957). The toxic effect of sodium L-glutamate on the inner layers of the retina. *Arch Opthalmol* **58**, 193–201.

Manabe S, Gu Z & Lipton SA (2005). Activation of matrix metalloproteinase-9 via neuronal nitric oxide synthase contributes to NMDA-induced retinal ganglion cell death. *Invest Ophthalmol Vis Sci* **46**, 4747–4753.

Manev H, Favaron M, Guidotti A & Costa E (1989). Delayed increase of Ca^{2+} influx elicited by glutamate: role in neuronal death. *Mol Pharmacol* **36**, 106–112.

Marc RE (1999*a*). Kainate activation of horizontal, bipolar, amacrine, and ganglion cells in the rabbit retina. *J Comp Neurol* **407**, 65–76.

Marc RE (1999*b*). Mapping glutamatergic drive in the vertebrate retina with a channel-permeant organic cation. *J Comp Neurol* **407**, 47–64.

Marc RE & Jones BW (2002). Molecular phenotyping of retinal ganglion cells. *J Neurosci* **22**, 413–427.

Mayer ML & Westbrook GL (1987). Permeation and block of N-methyl-D-aspartic acid receptor channels by divalent cations in mouse cultured central neurones. *J Physiol* **394**, 501–527.

Mayer ML, Westbrook GL & Guthrie PB (1984). Voltage-dependent block by Mg^{2+} of NMDA responses in spinal cord neurones. *Nature* **309**, 261–263.

Melena J & Osborne NN (2001). Voltage-dependent calcium channels in the rat retina: involvement in NMDA-stimulated influx of calcium. *Exp Eye Res* **72**, 292–401.

Meyer-Franke A, Kaplan MR, Pfrieger FW & Barres BA (1995). Characterization of the signaling interactions that promote the survival and growth of developing retinal ganglion cells in culture. *Neuron* **15**, 805–819.

Nakazawa T, Shimura M, Endo S, Takahashi H, Mori N & Tamai M (2005). N-Methyl-D-aspartic acid suppresses Akt activity through protein phosphatase in retinal ganglion cells. *Mol Vis* **11**, 1173–1182.

Nowak L, Bregestovski P, Ascher P, Herbet A & Prochiantz A (1984). Magnesium gates glutamate-activated channels in mouse central neurones. *Nature* **307**, 462–465.

Olney JW (1969). Glutamate-induced retinal degeneration in neonatal mice. Electron microscopy of the acutely evolving lesion. *J Neuropathol Exp Neurol* **28**, 455–474.

Osborne NN, Casson RJ, Wood JP, Chidlow G, Graham M & Melena J (2004). Retinal ischemia: mechanisms of damage and potential therapeutic strategies. *Prog Retin Eye Res* **23**, 91–147.

Osswald IK, Galan A & Bowie D (2007). Light triggers expression of philanthotoxin-insensitive Ca^{2+}-permeable AMPA receptors in the developing rat retina. *J Physiol* **582**, 95–111.

Otori Y, Wei JY & Barnstable CJ (1998). Neurotoxic effects of low doses of glutamate on purified rat retinal ganglion cells. *Invest Ophthalmol Vis Sci* **39**, 972–981.

Pernet V, Bourgeois P & Polo AD (2007). A role for polyamines in retinal ganglion cell excitotoxic death. *J Neurochem* **103**, 1481–1490.

Perry SW, Norman JP, Litzburg A & Gelbard HA (2004). Antioxidants are required during the early critical period, but not later, for neuronal survival. *J Neurosci Res* **78**, 485–492.

Potts RA, Dreher B & Bennett MR (1982). The loss of ganglion cells in the developing retina of the rat. *Brain Res* **255**, 481–486.

Rajdev S & Reynolds IJ (1994). Glutamate-induced intracellular calcium changes and neurotoxicity in cortical neurons in vitro: effect of chemical ischemia. *Neuroscience* **62**, 667–679.

Randall RD & Thayer SA (1992). Glutamate-induced calcium transient triggers delayed calcium overload and neurotoxicity in rat hippocampal neurons. *J Neurosci* **12**, 1882–1895.

Reichstein D, Ren L, Filippopoulos T, Mittag T & Danias J (2007). Apoptotic retinal ganglion cell death in the DBA/2 mouse model of glaucoma. *Exp Eye Res* **84**, 13–21.

Reynolds IJ & Hastings TG (1995). Glutamate induces the production of reactive oxygen species in cultured forebrain neurons following NMDA receptor activation. *J Neurosci* **15**, 3318–3327.

Sagdullaev BT, McCall MA & Lukasiewicz PD (2006). Presynaptic inhibition modulates spillover, creating distinct dynamic response ranges of sensory input. *Neuron* **50**, 923–935.

Sattler R, Charlton MP, Hafner M & Tymianski M (1998). Distinct influx pathways, not calcium load, determine neuronal vulnerability to calcium neurotoxicity. *J Neurochem* **71**, 2349–2364.

Sattler R & Tymianski M (2000). Molecular mechanisms of calcium-dependent excitotoxicity. *J Mol Med* **78**, 3–13.

Schlamp CL, Johnson EC, Li Y, Morrison JC & Nickells RW (2001). Changes in Thy1 gene expression associated with damaged retinal ganglion cells. *Mol Vis* **7**, 192–201.

Schmid S & Guenther E (1999). Voltage-activated calcium currents in rat retinal ganglion cells in situ: changes during prenatal and postnatal development. *J Neurosci* **19**, 3486–3494.

Schubert T & Akopian A (2004). Actin filaments regulate voltage-gated ion channels in salamander retinal ganglion cells. *Neuroscience* **125**, 583–590.

Siliprandi R, Canella R, Carmignoto G, Schiavo N, Zanellato A, Zanoni R & Vantini G (1992). N-methyl-D-aspartate-induced neurotoxicity in the adult rat retina. *Vis Neurosci* **8**, 567–573.

Sisk DR & Kuwabara T (1985). Histologic changes in the inner retina of albino rats following intravitreal injection of monosodium L-glutamate. *Graefes Arch Clin Exp Ophthalmol* **223**, 250–258.

Stout AK & Reynolds IJ (1999). High-affinity calcium indicators underestimate increases in intracellular calcium concentrations associated with excitotoxic glutamate stimulations. *Neuroscience* **89**, 91–100.

Sucher NJ, Aizenman E & Lipton SA (1991). N-methyl-D-aspartate antagonists prevent kainate neurotoxicity in rat retinal ganglion cells in vitro. *J Neurosci* **11**, 966–971.

Sucher NJ, Kohler K, Tenneti L, Wong HK, Grunder T, Fauser S, Wheeler-Schilling T, Nakanishi N, Lipton SA & Guenther E (2003). N-methyl-D-aspartate receptor subunit NR3A in the retina: developmental expression, cellular localization, and functional aspects. *Invest Ophthalmol Vis Sci* **44**, 4451–4456.

Sun D, Rait JL & Kalloniatis M (2003). Inner retinal neurons display differential responses to N-methyl-D-aspartate receptor activation. *J Comp Neurol* **465**, 38–56.

Taschenberger H, Engert F & Grantyn R (1995). Synaptic current kinetics in a solely AMPA-receptor-operated glutamatergic synapse formed by rat retinal ganglion neurons. *J Neurophysiol* **74**, 1123–1136.

Thoreson WB & Witkovsky P (1999). Glutamate receptors and circuits in the vertebrate retina. *Prog Retin Eye Res* **18**, 765–810.

Tymianski M, Charlton MP, Carlen PL & Tator CH (1993). Source specificity of early calcium neurotoxicity in cultured embryonic spinal neurons. *J Neurosci* **13**, 2085–2104.

Ullian EM, Barkis WB, Chen S, Diamond JS & Barres BA (2004). Invulnerability of retinal ganglion cells to NMDA excitotoxicity. *Mol Cell Neurosci* **26**, 544–557.

Ullian EM, Sapperstein SK, Christopherson KS & Barres BA (2001). Control of synapse number by glia. *Science* **291**, 657–661.

Wong WT, Myhr KL, Miller ED & Wong RO (2000). Developmental changes in the neurotransmitter regulation of correlated spontaneous retinal activity. *J Neurosci* **20**, 351–360.

Yang XL (2004). Characterization of receptors for glutamate and GABA in retinal neurons. *Prog Neurobiol* **73**, 127–150.

Zhang J & Diamond JS (2006). Distinct perisynaptic and synaptic localization of NMDA and AMPA receptors on ganglion cells in rat retina. *J Comp Neurol* **498**, 810–820.

Acknowledgements

This work was supported by an operating grant from the Canadian Institutes for Health Research (CIHR) to W.H.B. A.T.E.H. was an E. A. Baker Fellow, cosponsored by CIHR and the Canadian National Institute for the Blind, and a W. C. Ezell Fellow, sponsored by Bausch & Lomb through the American Optometric Foundation. We thank Tim Maillet for technical assistance.

Supplemental material

Online supplemental material for this paper can be accessed at:
http://jp.physoc.org/cgi/content/full/jphysiol.2008.154609/DC1
and
http://www.blackwell-synergy.com/doi/suppl/10.1113/jphysiol.2008.154609